NATIONAL ADVISORY COMMITTEE FOR AERONAUTICS

TECHNICAL NOTE 4390

EFFECTS OF FREQUENCY AND AMPLITUDE ON THE YAWING DERIVATIVES OF TRIANGULAR, SWEPT, AND UNSWEPT WINGS AND OF A TRIANGULAR-WING—FUSELAGE COMBINATION WITH AND WITHOUT A TRIANGULAR TAIL PERFORMING SINUSOIDAL YAWING OSCILLATIONS

By William Letko and Herman S. Fletcher

Langley Aeronautical Laboratory
Langley Field, Va.

Washington
September 1958

NATIONAL ADVISORY COMMITTEE FOR AERONAUTICS

TECHNICAL NOTE 4390

EFFECTS OF FREQUENCY AND AMPLITUDE ON THE YAWING DERIVATIVES OF TRIANGULAR, SWEPT, AND UNSWEPT WINGS AND OF A TRIANGULAR-WING—FUSELAGE COMBINATION WITH AND WITHOUT A TRIANGULAR TAIL PERFORMING SINUSOIDAL YAWING OSCILLATIONS

By William Letko and Herman S. Fletcher

SUMMARY

An investigation has been made to determine the effects of frequency and amplitude on the yawing derivatives of triangular, swept, and unswept wings. Some data were also obtained for a triangular-wing—fuselage combination with and without a triangular tail performing sinusoidal yawing oscillations. The oscillation data were compared with data obtained from steady-state yawing tests and the results of the present investigation and those of a pure sideslip investigation are compared both individually and as an algebraic sum with the combination derivatives obtained from an investigation in which the oscillation was a combination of yawing and sideslipping.

The results of the present investigation indicate that for the triangular wing, the 45° swept wing, and the wing-fuselage configuration, the oscillatory values of the damping-in-yaw derivative and the derivative of rolling moment due to yawing increased with angle of attack; generally, at the high angles of attack the oscillatory values were considerably larger than the steady-state values, especially for low amplitudes and low frequencies of oscillation. For the unswept wing there was generally little difference between the steady-state values and the oscillatory values of the damping-in-yaw derivative and the derivative of rolling moment due to yawing in the low angle-of-attack range; at higher angles of attack, the steady-state values usually were greater than the oscillatory values. Although for the complete wing-fuselage-tail model the variation of the oscillatory damping-in-yaw derivatives with angle of attack was similar generally to the steady-state variation, some oscillatory values were obtained which were four to five times greater than the steady-state values throughout the angle-of-attack range. The effects of amplitude on the yawing derivatives, although small at low angles of attack, became greater at the higher angles of attack; and the greatest effects occurred at low values of amplitude and frequency. The algebraic summation of the component derivatives gave results which were, in general, in fair agreement with the derivatives obtained in the combined form.

INTRODUCTION

Current airplanes of relatively high density have brought into consideration the importance of some factors associated with the dynamic stability of aircraft which heretofore were considered negligible. Among the factors are the effects of frequency and amplitude on stability derivatives and the possibility that acceleration derivatives may be of such magnitude as to be important for certain airplane configurations.

Some data to help assess the importance of these factors have already been obtained experimentally by use of oscillation techniques from which combination derivatives were obtained and are presented, for example, in references 1 to 3. Some investigations using a somewhat more complicated technique have resulted in direct measurement of the sideslip-acceleration derivatives (ref. 4) and have also resulted in the evaluation of the derivatives associated with sideslip velocity during a sinusoidal sideslip oscillation.

The investigation presented in reference 5 was made to determine the stability derivatives associated with yawing velocity and acceleration for one frequency and amplitude of oscillation. The present investigation was undertaken to extend the results of reference 5 to other frequencies and amplitudes of oscillation.

Oscillatory derivatives were obtained in the present investigation for triangular, swept, and unswept wings. In addition, some data were obtained for a triangular-wing—fuselage combination with and without a triangular tail. The oscillation data are compared with data obtained from steady-state yawing tests made in the 6- by 6-foot curved-flow test section of the Langley stability tunnel. In addition, the results of the present investigation and of additional tests similar to those presented in reference 4 are compared both individually and as an algebraic sum with the combination derivatives determined in reference 6.

SYMBOLS

The data presented are referred to the stability system of axes with the origin located at the quarter-chord of the wing mean aerodynamic chord. The positive directions of forces, moments, and angular displacements are shown in figure 1. The coefficients and symbols are defined as follows:

C_L lift coefficient, $\frac{\text{Lift}}{qS}$

C_l rolling-moment coefficient, $\frac{\text{Rolling moment}}{qSb}$

C_n yawing-moment coefficient, $\frac{\text{Yawing moment}}{qSb}$

M_X rolling moment, ft-lb

M_Z yawing moment, ft-lb

b wing span, ft

c wing chord, ft

$\bar{c}$ wing mean aerodynamic chord, $\frac{2}{S}\int_0^{b/2} c^2 dy$, ft

f frequency, cps

I_Z model moment of inertia about Z-axis, slug-ft^2

I_{XZ} product of inertia, slug-ft^2

l distance between flywheel centers, ft

e length of link arm from model center of gravity to push-rod pivot point (see fig. 2)

e' length of link arm from pivot point on flywheel to push-rod pivot point (see fig. 2), ft

q dynamic pressure, $\frac{1}{2}\rho V^2$, lb/sq ft

r angular velocity in yaw ($r = \dot{\psi}$), radians/sec

R throw of flywheels of oscillating mechanism (see fig. 2), ft

S wing surface area, sq ft

t time, sec

V free-stream velocity, ft/sec

y distance along Y-axis measured from wing plane of symmetry, ft

$\dot{y} = \frac{\partial y}{\partial t}$

y' distance between model mounting point and center of drive flywheel, ft

$\dot{y}' = \frac{\partial y'}{\partial t}$

α angle of attack, deg

β angle of sideslip, radians

β_o maximum amplitude of sideslip, deg

ψ angle of yaw, radians

ψ_o maximum amplitude of yaw, deg

k reduced-frequency parameter, $\frac{\omega b}{2V}$

ω circular frequency, radians/sec

ρ mass density of air, slugs/cu ft

$\dot{\beta} = \frac{\partial \beta}{\partial t}$

$\dot{r} = \frac{\partial r}{\partial t}$

$\dot{\psi} = \frac{\partial \psi}{\partial t}$

$\ddot{\psi} = \frac{\partial^2 \psi}{\partial t^2}$

$M_{X\dot{\psi}} = \frac{\partial M_X}{\partial \dot{\psi}}$

$$M_{X\ddot{\psi}} = \frac{\partial M_X}{\partial \ddot{\psi}}$$

$$M_{Z\dot{\psi}} = \frac{\partial M_Z}{\partial \dot{\psi}}$$

$$C_{l_\beta} = \frac{\partial C_l}{\partial \beta}$$

$$C_{l_{\dot{\beta}}} = \frac{\partial C_l}{\partial \frac{\dot{\beta} b}{2V}}$$

$$C_{n_\beta} = \frac{\partial C_n}{\partial \beta}$$

$$C_{n_{\dot{\beta}}} = \frac{\partial C_n}{\partial \frac{\dot{\beta} b}{2V}}$$

$$C_{l_r} = \frac{\partial C_l}{\partial \frac{rb}{2V}}$$

$$C_{l_{\dot{r}}} = \frac{\partial C_l}{\partial \frac{\dot{r} b^2}{4V^2}}$$

$$C_{n_r} = \frac{\partial C_n}{\partial \frac{rb}{2V}}$$

$$C_{n_{\dot{r}}} = \frac{\partial C_n}{\partial \frac{\dot{r} b^2}{4V^2}}$$

All the aforementioned derivatives are nondimensionalized in this paper (per radian).

The symbol ω following the subscript of a derivative denotes the oscillatory derivative.

APPARATUS

The tests of the present investigation were conducted in the 6- by 6-foot test section of the Langley stability tunnel. The oscillation equipment was designed to generate an oscillatory motion in the XY-plane so that the airplane would always be heading into the relative wind or, more specifically, so that there would be no resultant lateral velocity component at the airplane center of gravity. The following sketch illustrates the path and attitude of an airplane performing a pure sinusoidal yawing oscillation:

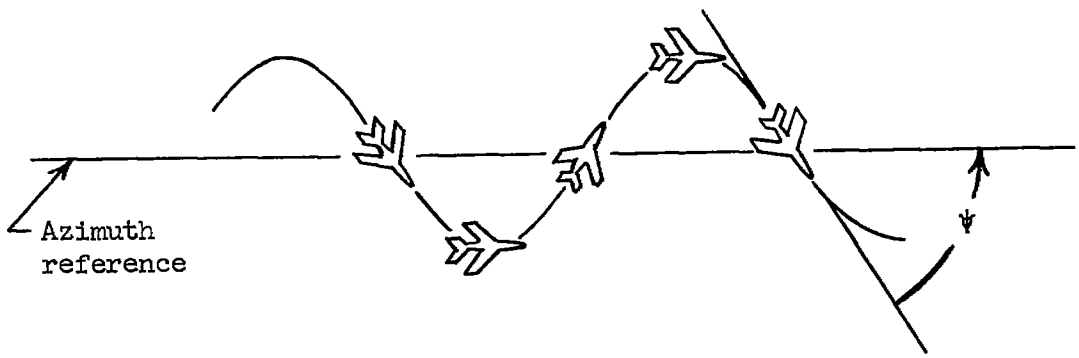

The condition of no lateral resultant velocity at the assumed model center of gravity or mounting point is fulfilled when $V \sin \psi = \dot{y}$. For small angular motions of the model this condition can be written as $V\psi = \dot{y}$ and was approximated in the present investigation by use of the apparatus shown schematically in figure 2. Photographs of the actual apparatus are given as figure 3.

The main components of the apparatus used in the present investigation were also used in the investigation in reference 5. For the present tests the apparatus differed from that used in reference 5 in that provision was made so that the model could be pivoted in yaw with respect to the streamline tube. The resulting angle of yaw of the model was, therefore, different from that which would result if the model were rigidly attached to the streamline tube. The motion of the model with respect to the streamline tube could be regulated by means of the adjustable linkages shown in figures 2 and 3. The streamline

tube was supported on the ends by opposite rotating flywheels, which were driven by means of various shafts, gears, and a variable-frequency motor-generator set. The yaw angle of the model at any instant, if small angular motions of the model are assumed, is given by

$$\psi = \left(\frac{2R}{l} - \frac{e'}{e}\right) \sin 2\pi ft$$

The distance between the model mounting point and the center of the drive flywheel is $y' = \frac{l}{2} \cos \psi + R \cos 2\pi ft$. For small angular displacements of the model, $y' = \frac{l}{2} + R \cos 2\pi ft$; hence, the velocity of the model toward the drive flywheel is $\dot{y}' = -2\pi fR \sin 2\pi ft$ which for small angular motions can be taken to be the sideslip velocity $\dot{y}$. For a pure yawing oscillation the relation between V and f is then

$$V = \frac{-2\pi fR \sin 2\pi ft}{\left(\frac{2R}{l} - \frac{e'}{e}\right) \sin 2\pi ft}$$

$$= - \frac{2\pi fR}{\frac{2R}{l} - \frac{e'}{e}}$$

or

$$f = - \frac{V}{2\pi R}\left(\frac{2R}{l} - \frac{e'}{e}\right)$$

Therefore, for a given velocity and a given distance between flywheels, proper conditions for the required motion could be obtained at different frequencies by adjusting R, e', and e.

The yawing and rolling moments acting on the models during the tests were measured by means of a strain-gage balance. The signals from the strain gage were passed into the instrumentation which permitted direct measurements of quantities proportional to the moments due to yawing velocity and acceleration. A description of the design and function of the instrumentation is given in the appendix of reference 5.

MODELS

The wing models used in this investigation were those previously used in the investigations presented in references 4 and 5 and consisted

of a 60° triangular, a 45° sweptback, and an unswept wing. The swept and unswept wings had an aspect ratio of 4.0 and a taper ratio of 0.6. The aspect ratio of the triangular wing was 2.31. Each wing was constructed from 3/4-inch plywood and had a flat-plate airfoil section with a circular leading edge and a beveled trailing edge. The trailing edges of all wings were beveled to provide a trailing-edge angle of 10° across the span. Sketches of the three wings and their geometric characteristics are presented in figure 4.

The complete-model configuration used in the present tests was one used previously in the investigation presented in reference 7. The configuration consisted of a removable triangular wing with an aspect ratio of 2.31, a fuselage with a fineness ratio of 9, and a triangular vertical tail with an aspect ratio of 2.18. The wing was a 60° triangular wing and had an NACA 65A003 profile in sections parallel to the plane of symmetry. The tail had 42.5° of sweep of the leading edge and had an NACA 65-006 profile in sections parallel to the fuselage center line. A sketch of the complete model is presented as figure 5, and its geometric characteristics are given in table I. Table II presents the coordinates of the fuselage.

Before testing the models, each wing was lightened and statically balanced about the mounting point to reduce inertia effects insofar as possible. A fairing which was used for the wing-alone tests was made of balsa and served to streamline the protrusion of the strain-gage balance above the upper surface of the models at angles of attack. All openings in the canopies were sealed to prevent leakage of air through the model.

TESTS AND CORRECTIONS

All tests of this investigation were made in the 6- by 6-foot test section of the Langley stability tunnel. The oscillation tests were made at a dynamic pressure of 24.9 pounds per square foot. The reduced-frequency parameter $\frac{\omega b}{2V}$ of the tests varied from 0.04 to 0.20, and the maximum amplitude of yaw ψ_o varied from ±0.67° to ±6.11°.

The Reynolds number of the tests, based on the wing mean aerodynamic chord, and the angle-of-attack range for each model were as follows:

Model	Reynolds number, based on $\bar{c}$	Angle-of-attack range, deg
60° triangular wing	1,580,000	0 to 32
45° sweptback wing.	696,000	0 to 32
Unswept wing	696,000	0 to 16
Triangular-wing—fuselage combination	1,580,000	0 to 32
Triangular-wing—fuselage combination with triangular vertical tail	1,580,000	0 to 32

No jet-boundary corrections were applied to the data nor were the effects of blockage, turbulence, or support interference taken into account although the support interference may be of sizeable magnitude at the higher angles of attack.

REDUCTION OF OSCILLATION-TEST DATA

The equations of motion for a model performing a forced sinusoidal yawing oscillation about the Z-axis and X-axis, respectively, are

$$M_{Z\psi}\psi + M_{Z\dot{\psi}}\ddot{\psi} + B \sin 2\pi ft + C \cos 2\pi ft = I_Z\ddot{\psi}$$

and

$$M_{X\psi}\psi + M_{X\dot{\psi}}\ddot{\psi} + D \sin 2\pi ft + E \cos 2\pi ft = -I_{XZ}\ddot{\psi}$$

where B and D are the maximum in-phase yawing and rolling moments, respectively, and C and E are the corresponding out-of-phase yawing and rolling moments supplied by the strain gage. The yaw angle for the present tests, if small yaw angles are assumed, is given by

$$\psi = \left(\frac{2R}{l} - \frac{e'}{e}\right)\sin 2\pi ft$$

By using the equations of motion and this relationship for the yaw angle, the subsequent expressions for the oscillatory derivatives are obtained by following the procedures outlined in reference 5:

$$C_{n_r} = \frac{2\left(C_{\text{wind on}} - C_{\text{wind off}}\right)}{\pi f\left(\frac{2R}{l} - \frac{e'}{e}\right)\rho V S b^2}$$

$$C_{l_r} = \frac{2\left(E_{\text{wind on}} - E_{\text{wind off}}\right)}{\pi f\left(\frac{2R}{l} - \frac{e'}{e}\right)\rho V S b^2}$$

$$C_{n_{\dot{r}}} = \frac{-2\left(B_{\text{wind on}} - B_{\text{wind off}}\right)}{\pi^2 f^2\left(\frac{2R}{l} - \frac{e'}{e}\right)\rho S b^3}$$

$$C_{l_{\dot{r}}} = \frac{-2\left(D_{\text{wind on}} - D_{\text{wind off}}\right)}{\pi^2 f^2\left(\frac{2R}{l} - \frac{e'}{e}\right)\rho S b^3}$$

In the present tests the moments B, C, D, and E were determined from voltage measurements by the electronic equipment described in the appendix of reference 5. As shown in the appendix of reference 5, the instrumentation used in this investigation yielded readings on a voltmeter which were directly proportional to one-half of the yawing and rolling moments; hence, the aerodynamic moments B, C, D, and E could be obtained readily and the derivatives could be determined by use of the equations previously presented.

RESULTS AND DISCUSSION

In figures 6 and 7 are shown the lift data plotted against angle of attack for the three wings and wing-fuselage-tail combination, respectively. These data have been presented and discussed in references 4 and 7, respectively, and are not discussed herein but are included primarily to relate the lift to angle of attack.

The data measured during oscillation tests are presented in figures 8 to 17. In figures 18 to 21 the wing-alone results of the present investigation are compared with data obtained from sideslipping tests similar to those presented in reference 4. In addition, the derivatives are compared as an algebraic sum with the combination derivatives determined in reference 6.

Damping in Yaw $C_{n_{r,\omega}}$

Wings alone.- The variation of the damping-in-yaw characteristics with angle of attack for the wings alone is given in figures 8, 9, and 10 for different amplitudes and different values of reduced-frequency parameter $\frac{\omega b}{2V}$. For the 60° triangular wing (fig. 8) and for the 45° swept wing (fig. 9), the values of $C_{n_{r,\omega}}$ generally are small in the low angle-of-attack range but increase as the angle of attack is increased. This is especially true for the data obtained at $\frac{\omega b}{2V} = 0.04$. At the large angles of attack the oscillatory values of C_{n_r} also are considerably larger than the steady-state values of C_{n_r} which show a much smaller variation with angle of attack. The steady-state values of C_{n_r} obtained from reference 7 are shown by the dashed-line curve in each figure. For the unswept wing at the low values of amplitude and reduced-frequency parameter, the variation of $C_{n_{r,\omega}}$ with angle of attack is generally rather irregular (fig. 10); whereas for the large values of amplitude and reduced-frequency parameter the variation of $C_{n_{r,\omega}}$ with angle of attack is small. In fact, the variation of $C_{n_{r,\omega}}$ with angle of attack is smaller than the variation of the steady-state values, and at the high angles of attack the oscillatory values are positive or less negative than the steady-state values.

Figures 11, 12, and 13 are presented in order to show more clearly the variation with amplitude of the values of $C_{n_{r,\omega}}$ for the three wings. For all three wings these figures show that at low angles of attack there is only a small effect of amplitude on $C_{n_{r,\omega}}$ for all values of the reduced-frequency parameter shown. At the higher angles of attack the effect of amplitude on the values of $C_{n_{r,\omega}}$ is larger, the largest changes occurring in the low-amplitude range and at the low values of the reduced-frequency parameter.

Wing-fuselage configuration.- The variation of the damping in yaw $C_{n_{r,\omega}}$ with angle of attack for the triangular-wing—fuselage configuration is shown in figure 14 for different amplitudes and different values of the reduced-frequency parameter. In general, the values of $C_{n_{r,\omega}}$ become more negative (increased damping) with increase of angle of attack

for all test values of $\frac{\omega b}{2V}$; however, the increase with angle of attack is much less for the larger values of $\frac{\omega b}{2V}$. The steady-state values of C_{n_r} do not vary appreciably with angle of attack and are much less negative at the high angles of attack than the oscillatory values, the closest agreement occurring at the higher values of $\frac{\omega b}{2V}$.

The variations of the $C_{n_{r,\omega}}$ data with amplitude for the wing-fuselage configuration are shown in figure 15 for different values of $\frac{\omega b}{2V}$. Because of lack of sufficient data, the curves are faired only through the test points for $\frac{\omega b}{2V} = 0.08$. The effect of amplitude is generally small in the low angle-of-attack range but is much greater at the high angles of attack where the damping increases with amplitude. It should be pointed out, however, that the effects of amplitude on $C_{n_{r,\omega}}$ may be different for other frequencies of oscillation.

Wing-fuselage-tail configuration.- For the complete wing-fuselage-tail configuration, the variation of $C_{n_{r,\omega}}$ with angle of attack is shown in figure 16 for different frequencies and amplitudes of oscillation. Also included in this figure is the variation with angle of attack of the steady-state values of C_{n_r}. In general, the oscillatory values of $C_{n_{r,\omega}}$ are considerably more negative than the steady-state values. With few exceptions the values of the oscillatory derivatives are at least twice the steady-state values and, in some cases, the oscillatory values are as much as four and five times as large as the steady-state values. The largest differences occur usually for low values of amplitude and frequency.

As was the case for the wing-fuselage configuration, insufficient data were obtained to show the variation of $C_{n_{r,\omega}}$ with amplitude for the range of frequencies in the investigation. Therefore, in figure 17 a curve was faired only through the data obtained at $\frac{\omega b}{2V} = 0.08$. The faired data generally showed that $C_{n_{r,\omega}}$ becomes less negative (reduced damping) with an increase in amplitude. The results at a higher value of $\frac{\omega b}{2V}$ may be different but, as was mentioned before, not enough data were obtained to establish a definite trend.

Rolling Moment Due to Yawing $C_{l_{r,\omega}}$

Wings alone.- The variation of the rolling moment due to yawing with angle of attack of the wings alone is given in figures 8, 9, and 10 for different amplitudes and different values of the reduced-frequency parameter $\frac{\omega b}{2V}$. The values of $C_{l_{r,\omega}}$ increase rapidly with an increase in angle of attack for all three wings. The variation with angle of attack is generally nonlinear at low values of amplitude and low values of the reduced-frequency parameter but tends toward linearity at the higher values of amplitude and $\frac{\omega b}{2V}$. At high angles of attack the oscillatory values of C_{l_r} are considerably greater than the steady-state values for both the triangular and 45° swept wings regardless of frequency or amplitude; however, the difference between the steady-state values and the oscillatory values of C_{l_r} is much less at the higher values of amplitude and frequency. For the unswept wing at the higher angles of attack, however, the steady-state values are greater than the oscillatory values of C_{l_r} for the higher values of amplitude and $\frac{\omega b}{2V}$. For low values of $\frac{\omega b}{2V}$ at high angles of attack, values of $C_{l_{r,\omega}}$ are obtained which, depending on the amplitude of oscillation, are sometimes greater and sometimes less than the steady-state values.

The variation with amplitude of the rolling moment due to yawing of the three wings is shown in figures 11, 12, and 13. Generally, there is only a comparatively small effect of amplitude on $C_{l_{r,\omega}}$ at low angles of attack. The effects of amplitude are greater at the higher angles of attack, and generally greater changes in $C_{l_{r,\omega}}$ take place in the lower range of amplitudes.

Wing-fuselage and wing-fuselage-tail configurations.- The variation of the derivative $C_{l_{r,\omega}}$ with angle of attack for the triangular-wing—fuselage configuration with and without a tail (figs. 14 and 16, respectively) is very similar to that obtained with the triangular wing alone (fig. 8) since $C_{l_{r,\omega}}$ is mainly due to the wing. The relation between the steady-state values and the oscillatory values for the complete wing-fuselage-tail configuration and the wing-fuselage configuration is also similar to that obtained for the wing alone.

For both the wing-fuselage and wing-fuselage-tail configurations there appears to be a decrease in $C_{l_{r,\omega}}$ with an increase in amplitude

(figs. 15 and 17), and the greatest changes appear to take place at the lower values of amplitude; as before it should be pointed out that insufficient data have been obtained to make a general statement for all values of frequency.

Acceleration Derivatives $C_{n_{\dot{r},\omega}}$ and $C_{l_{\dot{r},\omega}}$

Wings alone.- The acceleration derivatives $C_{n_{\dot{r},\omega}}$ and $C_{l_{\dot{r},\omega}}$ plotted against angle of attack for the three wings tested are presented in figures 8, 9, and 10 for different frequencies and amplitudes of oscillation. In general, the derivatives are significant only at the lower frequencies and amplitudes of oscillation.

Wing-fuselage and wing-fuselage-tail configurations.- The variation with angle of attack of the acceleration derivatives for the wing-fuselage and wing-fuselage-tail configurations are shown in figures 14 and 16, respectively. In general, the values of $C_{n_{\dot{r},\omega}}$ tend to become more positive or less negative, and the values of $C_{l_{\dot{r},\omega}}$ tend to become less positive or more negative with an increase in angle of attack up to an angle of attack of about 16°. At higher angles of attack the variation appears to depend on amplitude and is rather irregular. At low angles of attack and low values of $\frac{\omega b}{2V}$ the effect of amplitude on $C_{n_{\dot{r},\omega}}$ is much greater for the complete configuration than it is for the wing-fuselage configuration.

In order to illustrate the variation of the acceleration derivatives with amplitude at several angles of attack, figures 15 and 17 were prepared which show more clearly the effect of amplitude mentioned. There is some scatter of the data points for the various frequencies from the curve faired for $\frac{\omega b}{2V} = 0.08$; however, there were not enough data points obtained at other values of $\frac{\omega b}{2V}$ to establish definite amplitude effects at the other frequencies.

Comparison of Yawing and Acceleration Derivatives With Combined Derivatives for Wings Alone

For purposes of comparison with the measured combination derivatives, the derivatives $C_{n_{r,\omega}}$, $C_{n_{\dot{r},\omega}}$, $C_{l_{r,\omega}}$, and $C_{l_{\dot{r},\omega}}$ measured in this

investigation at $\frac{\omega b}{2V} = 0.20$ and amplitudes corresponding to $\psi_o = \pm 1.91^\circ$ and $\pm 3.82^\circ$ are combined with derivatives $C_{n_{\beta,\omega}}$, $C_{n_{\dot{\beta},\omega}}$, $C_{l_{\beta,\omega}}$, and $C_{l_{\dot{\beta},\omega}}$ measured in a series of unpublished tests similar to those in reference 4. The unpublished tests were forced-oscillation tests with $\frac{\omega b}{2V}$ approximately equal to 0.22 and amplitudes of sideslip β_o equal to $\pm 2^\circ$ and $\pm 4^\circ$. These individual derivatives and their appropriate algebraic summations are compared in figures 18 to 21 with the corresponding combination derivatives obtained in reference 6 for $\frac{\omega b}{2V}$ approximately equal to 0.22 and at amplitudes of yaw ψ_o equal to $\pm 2^\circ$ and $\pm 4^\circ$. The agreement in the variation with angle of attack of the measured combined derivatives and those obtained by an algebraic summation of the individual derivatives is considered very good, whereas the agreement in magnitudes of the derivatives is considered fair. The comparison indicates also that for the combination derivatives $\left(C_{n_{r,\omega}} - C_{n_{\dot{\beta},\omega}}\right)$ and $\left(C_{l_{r,\omega}} - C_{l_{\dot{\beta},\omega}}\right)$ the acceleration terms contribute as much or more to the measured combination derivatives as the $C_{n_{r,\omega}}$ and $C_{l_{r,\omega}}$ portions for all three wings throughout the angle-of-attack range. Because of the fact that the acceleration terms $C_{n_{\dot{r},\omega}}$ and $C_{l_{\dot{r},\omega}}$ are multiplied by k^2, these terms contribute considerably less to the total derivative than do the other terms of the combined derivatives $\left(C_{n_{\beta,\omega}} + k^2 C_{n_{\dot{r},\omega}}\right)$ and $\left(C_{l_{\beta,\omega}} + k^2 C_{l_{\dot{r},\omega}}\right)$.

SUMMARY OF RESULTS

Triangular, swept, and unswept wings were tested to determine the effects of frequency and amplitude on the yawing derivatives. A triangular-wing—fuselage combination with and without a triangular tail performing sinusoidal yawing oscillations was also included in the investigation. The results of the investigation are as follows:

1. For the triangular wing, the 45° swept wing, and the wing-fuselage configuration, oscillatory values of the damping-in-yaw derivative and the derivative of rolling moment due to yawing increased with angle of attack; generally, at the high angles of attack the oscillatory values were considerably larger than the steady-state values. For the unswept wing there was generally little difference between the steady-state values and the oscillatory values of the damping-in-yaw derivative and

the derivative of rolling moment due to yawing in the low angle-of-attack range; at higher angles of attack, the steady-state values usually were greater than the oscillatory values.

2. Although the variation of the damping-in-yaw derivative with angle of attack was similar generally to the steady-state variation, for the triangular-wing—fuselage combination with vertical tail, some oscillatory values were obtained which were four to five times greater than the steady-state values throughout the angle-of-attack range.

3. The effects of amplitude on the yawing derivatives were small at low angles of attack for the wings alone. The effects of amplitude and frequency were greater at the higher angles of attack, and the largest effects occurred at low values of amplitude and frequency.

4. The algebraic summation of the derivatives showed trends with angle of attack which were in very good agreement with the variation shown by the measured combined derivatives. The agreement in magnitudes of the derivatives was considered fair.

Langley Aeronautical Laboratory,
National Advisory Committee for Aeronautics,
Langley Field, Va., April 28, 1958.

REFERENCES

1. Fisher, Lewis R., and Fletcher, Herman S.: Effect of Lag of Sidewash on the Vertical-Tail Contribution to Oscillatory Damping in Yaw of Airplane Models. NACA TN 3356, 1955.

2. Campbell, John P., Johnson, Joseph L., Jr., and Hewes, Donald E.: Low-Speed Study of the Effect of Frequency on the Stability Derivatives of Wings Oscillating in Yaw With Particular Reference to High Angle-of-Attack Conditions. NACA RM L55H05, 1955.

3. Johnson, Joseph L., Jr.: Low-Speed Measurements of Rolling and Yawing Stability Derivatives of a 60° Delta-Wing Model. NACA RM L54G27, 1954.

4. Riley, Donald R., Bird, John D., and Fisher, Lewis R.: Experimental Determination of the Aerodynamic Derivatives Arising From Acceleration in Sideslip for a Triangular, a Swept, and an Unswept Wing. NACA RM L55A07, 1955.

5. Queijo, M. J., Fletcher, Herman S., Marple, C. G., and Hughes, F. M.: Preliminary Measurements of the Aerodynamic Yawing Derivatives of a Triangular, a Swept, and an Unswept Wing Performing Pure Yawing Oscillations, With a Description of the Instrumentation Employed. NACA RM L55L14, 1956.

6. Fisher, Lewis R.: Experimental Determination of the Effects of Frequency and Amplitude on the Lateral Stability Derivatives for a Delta, a Swept, and an Unswept Wing Oscillating in Yaw. NACA RM L56A19, 1956.

7. Jaquet, Byron M., and Fletcher, Herman S.: Experimental Steady-State Yawing Derivatives of a 60° Delta-Wing Model As Affected by Changes in Vertical Position of the Wing and in Ratio of Fuselage Diameter to Wing Span. NACA TN 3843, 1956.

TABLE I.- GEOMETRIC CHARACTERISTICS OF COMPLETE-MODEL CONFIGURATION

Fuselage:	
Fineness ratio	9
Maximum diameter, in.	6.0
Wing:	
Aspect ratio	2.31
Leading-edge sweep angle, deg	60
Dihedral angle, deg	0
Twist, deg	0
NACA airfoil section parallel to plane of symmetry	65A003
Area, sq in.	576.7
Span, in.	36.50
Mean aerodynamic chord, in.	21.10
Vertical tail:	
Aspect ratio	2.18
Leading-edge sweep angle, deg	42.5
NACA airfoil section parallel to fuselage center line	65-006
Area for 12-inch span, sq in.	66.0
Tail length from center of gravity to 0.25 mean aerodynamic chord of tail, in.	21.5

TABLE II.- FUSELAGE COORDINATES

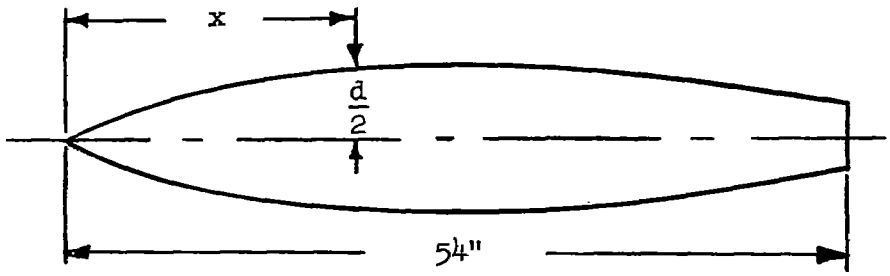

x, in.	$\frac{d}{2}$, in.
0	0
.324	.01918
.486	.1296
.810	.2214
1.620	.432
3.240	.8316
4.86	1.1988
6.48	1.5336
9.72	2.0898
12.96	2.5218
16.20	2.808
19.44	2.970
21.6	3.0024
22.68	2.9916
25.92	2.9808
29.16	2.9214
32.40	2.8296
35.64	2.7216
38.88	2.5704
42.12	2.3922
45.36	2.1924
48.60	1.9494
51.84	1.6902
54.0	1.4904

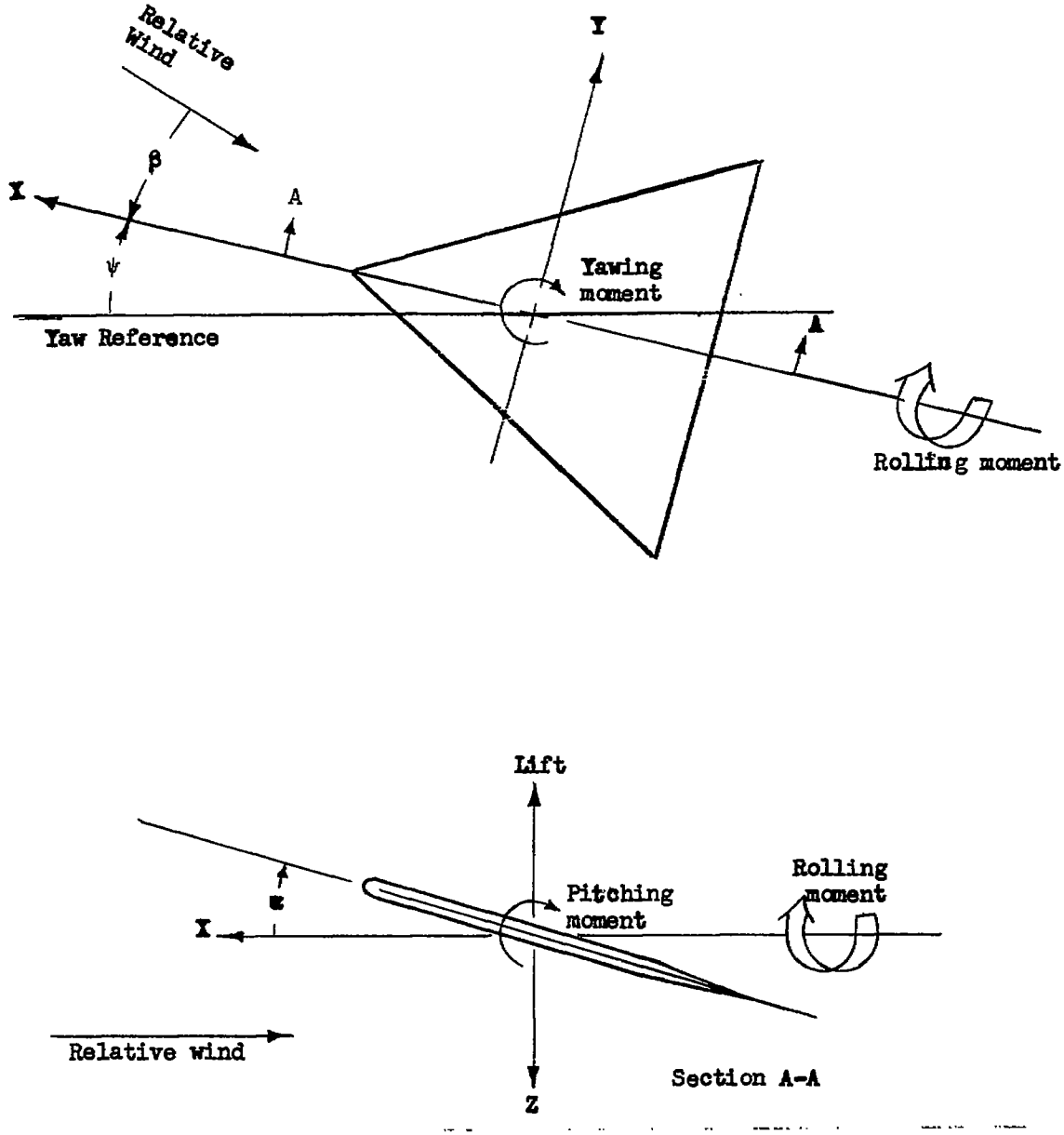

Figure 1.- System of stability axes. Arrows indicate positive forces, moments, and angular displacements. Yaw reference is generally chosen to coincide with initial relative wind.

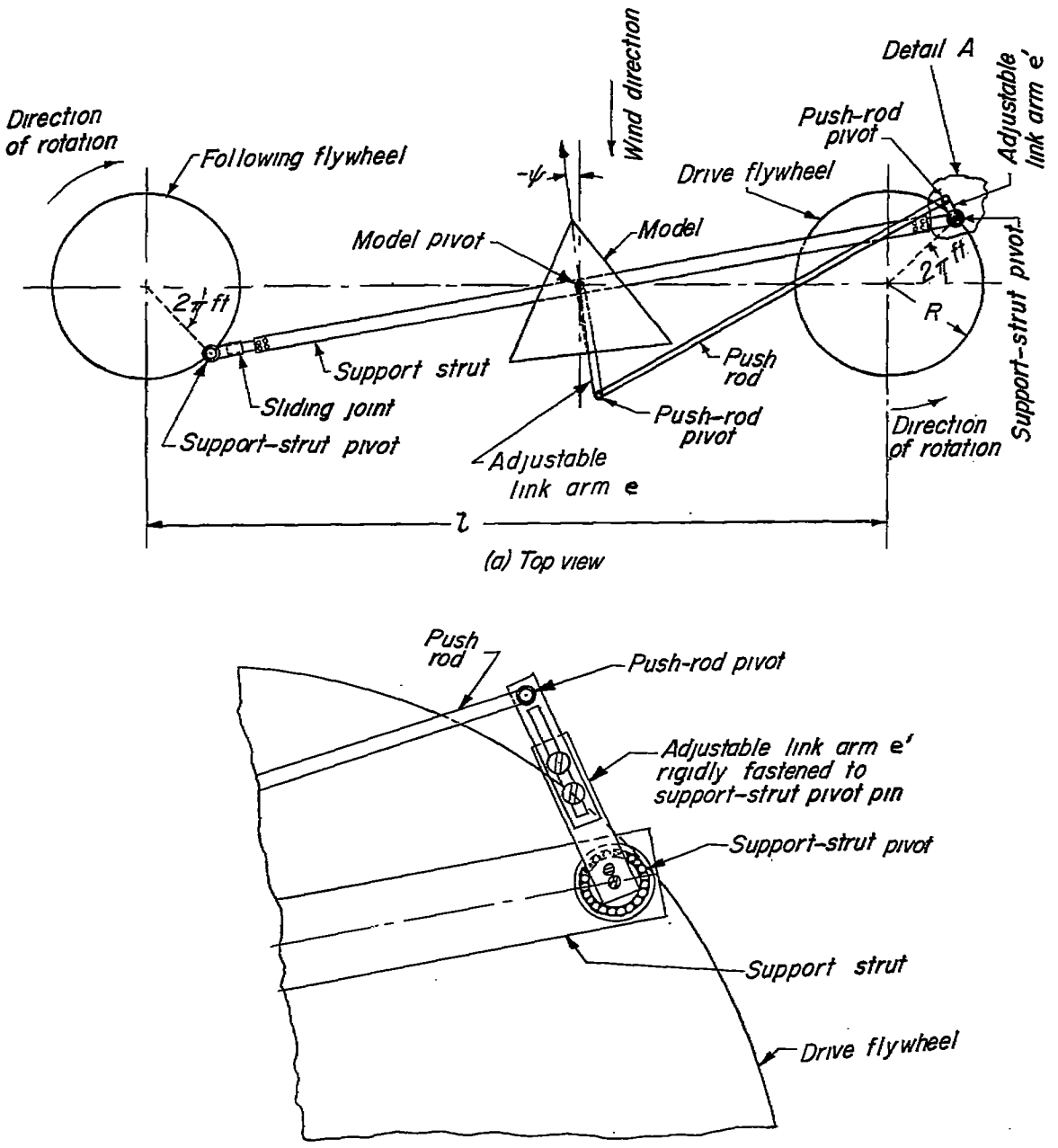

Figure 2.- Schematic drawing of mechanism for simulating sinusoidal yawing oscillation.

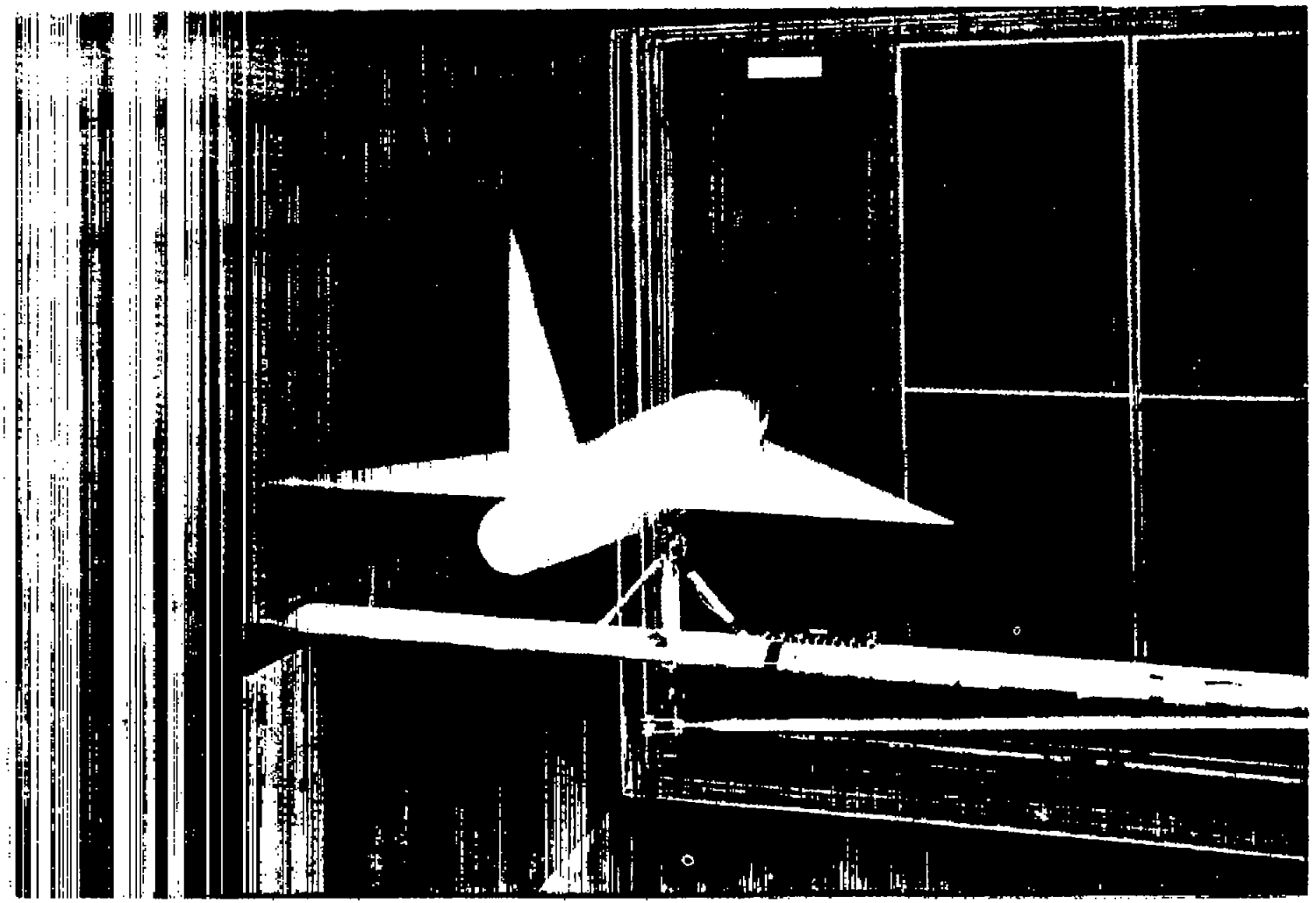

(a) Model support strut and complete-model configuration. L-94582

Figure 3.- Apparatus used in obtaining sinusoidal yawing oscillation.

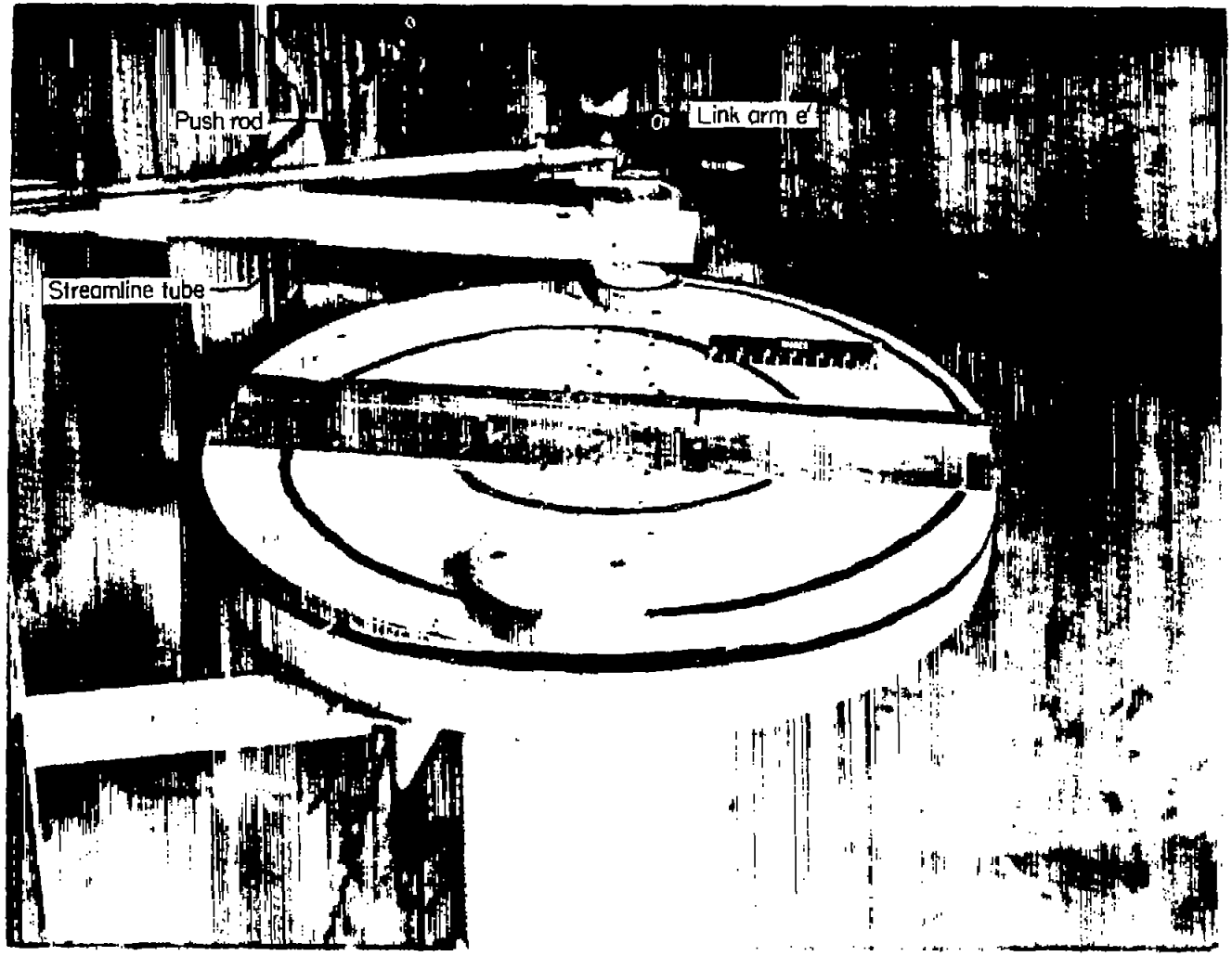

(b) Drive flywheel and linkages. L-94585.1

Figure 3.- Concluded.

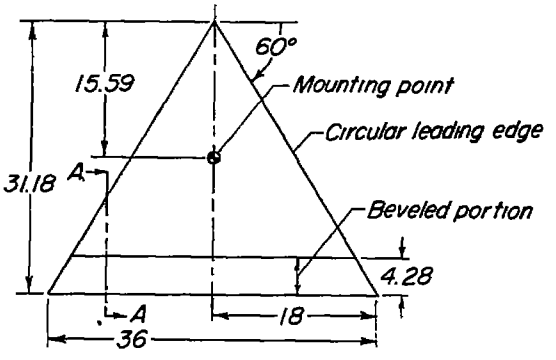

Triangular wing

Aspect ratio	2.31
Leading-edge sweep angle, deg	60
Dihedral angle, deg	0
Twist, deg	0
Airfoil section	Flat plate
Area, sq. in.	561.20
Span, in.	36.00
Mean aerodynamic chord, in.	20.79

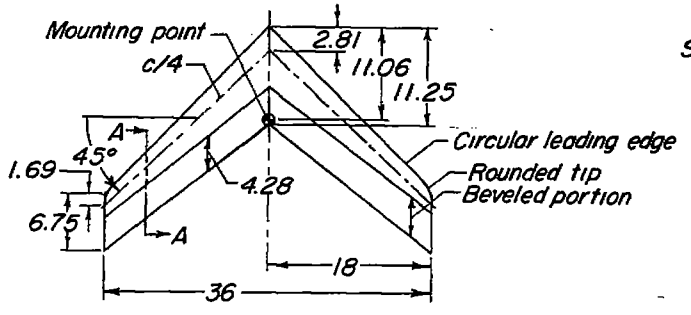

Swept wing

Aspect ratio	4.0
Taper ratio	0.6
Quarter-chord sweep angle, deg	45
Dihedral angle, deg	0
Twist, deg	0
Airfoil section	Flat plate
Area, sq. in.	324
Span, in.	36
Mean aerodynamic chord, in.	9.19

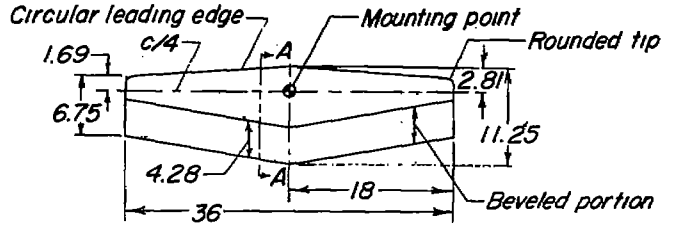

Unswept wing

Aspect ratio	4.0
Taper ratio	0.6
Quarter-chord sweep angle, deg	0
Dihedral angle, deg	0
Twist, deg	0
Airfoil section	Flat plate
Area, sq. in.	324
Span, in.	36
Mean aerodynamic chord, in.	9.19

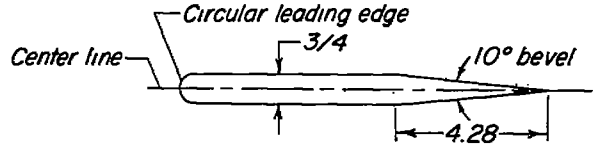

Section A-A

Figure 4.- Sketches and geometric characteristics of the three wing models investigated. All dimensions are in inches.

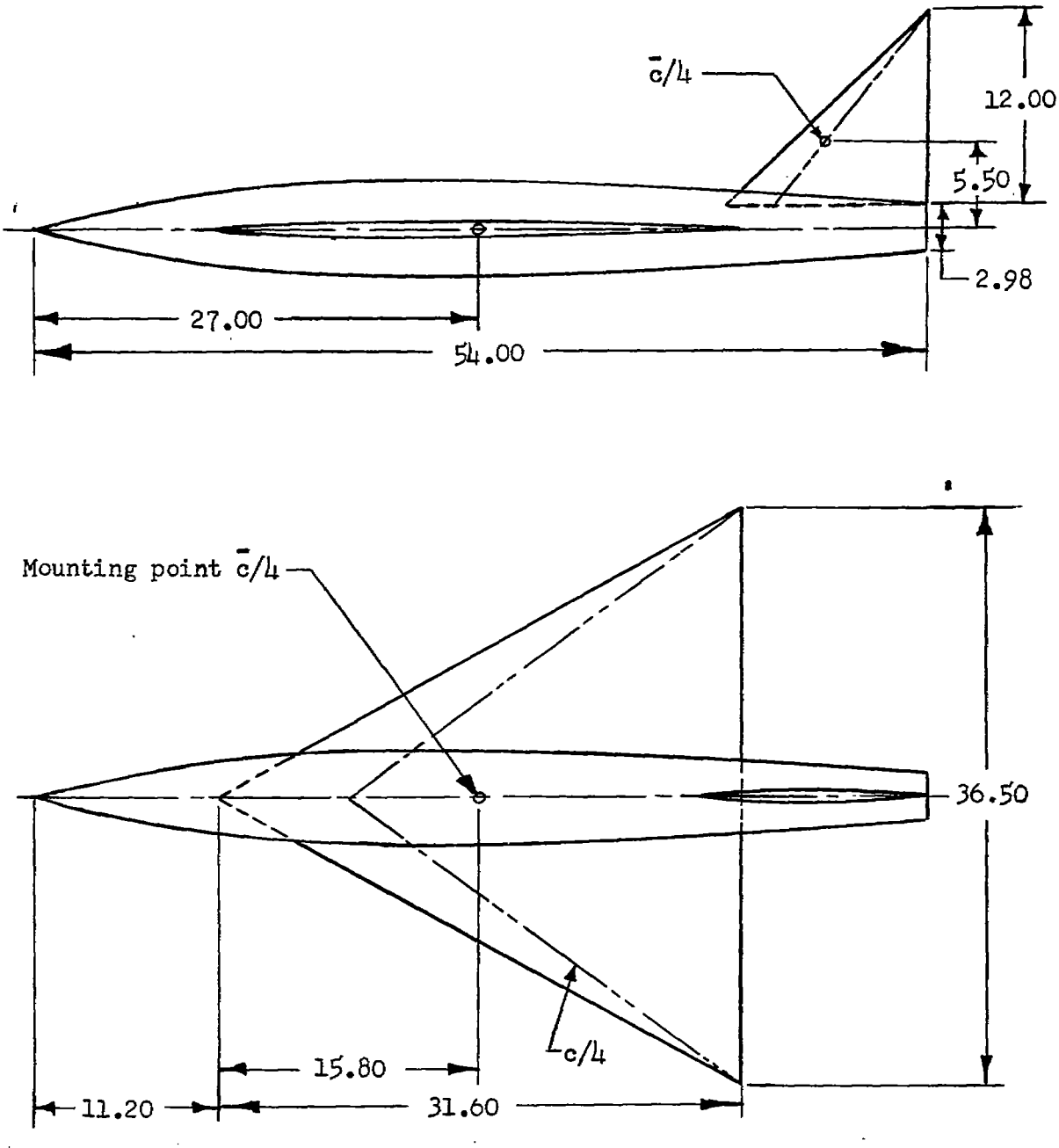

Figure 5.- Sketch of complete wing-fuselage-tail configuration. All dimensions are in inches.

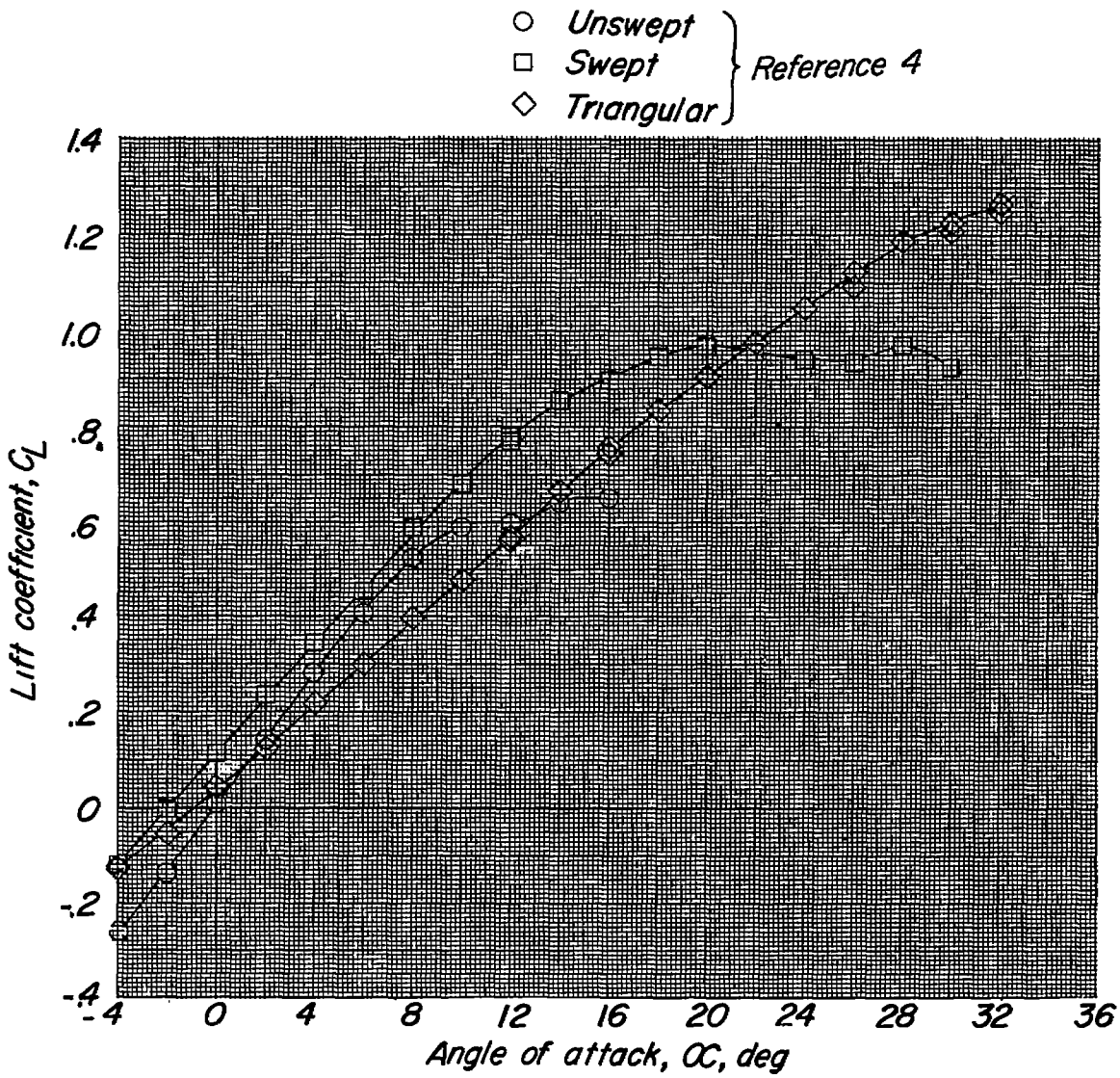

Figure 6.- Lift characteristics of wings used in investigation.

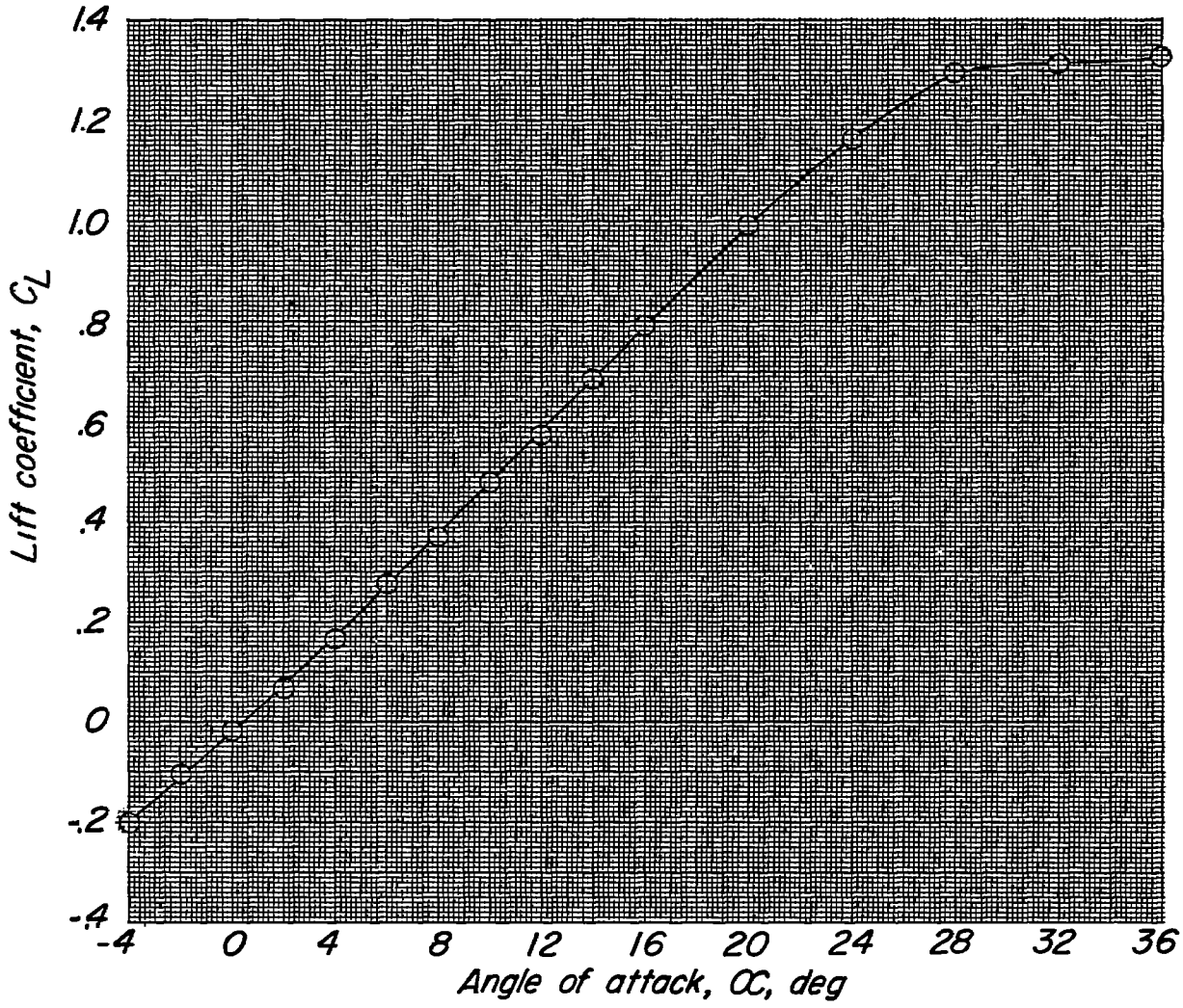

Figure 7.- Lift characteristics of wing-fuselage-tail configuration used in investigation. Data are taken from reference 7.

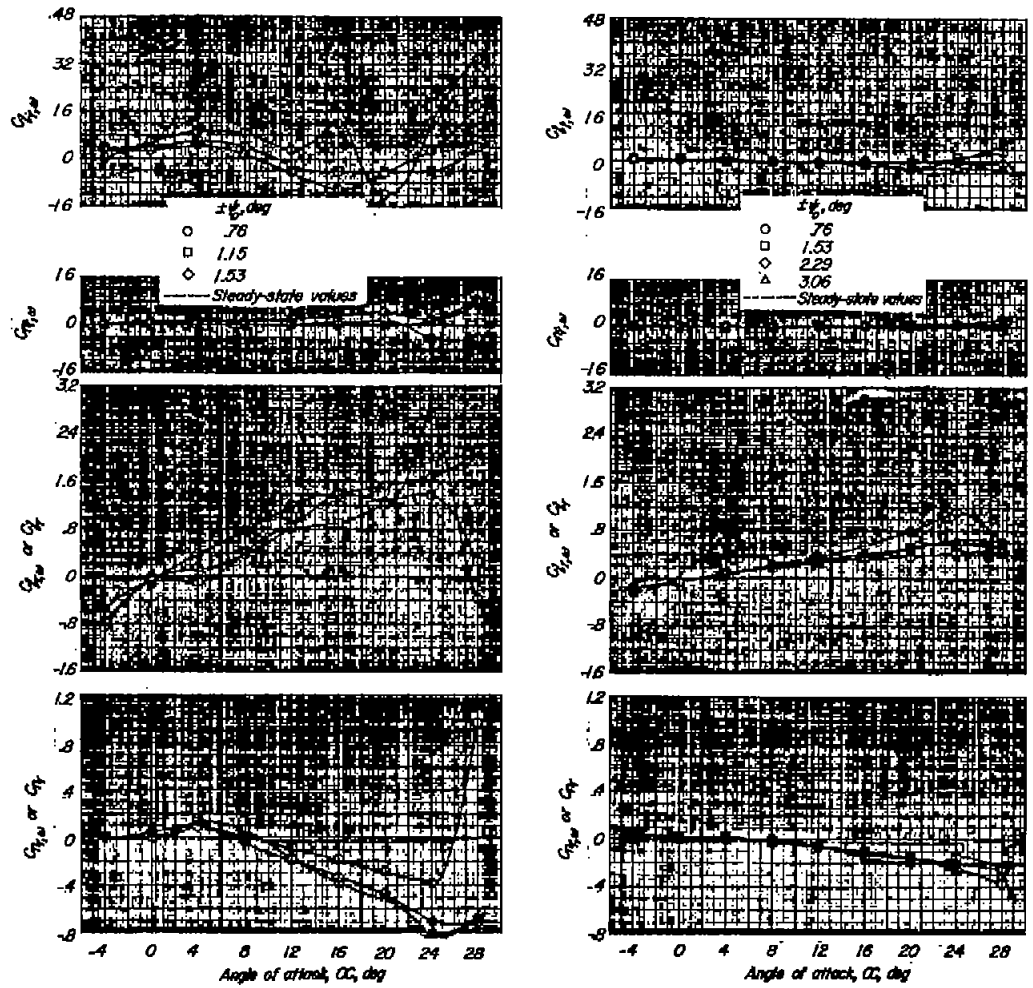

(a) $\frac{\omega b}{2V} = 0.04$.

(b) $\frac{\omega b}{2V} = 0.08$.

Figure 8.- Stability derivatives for the 60° triangular wing measured during oscillation.

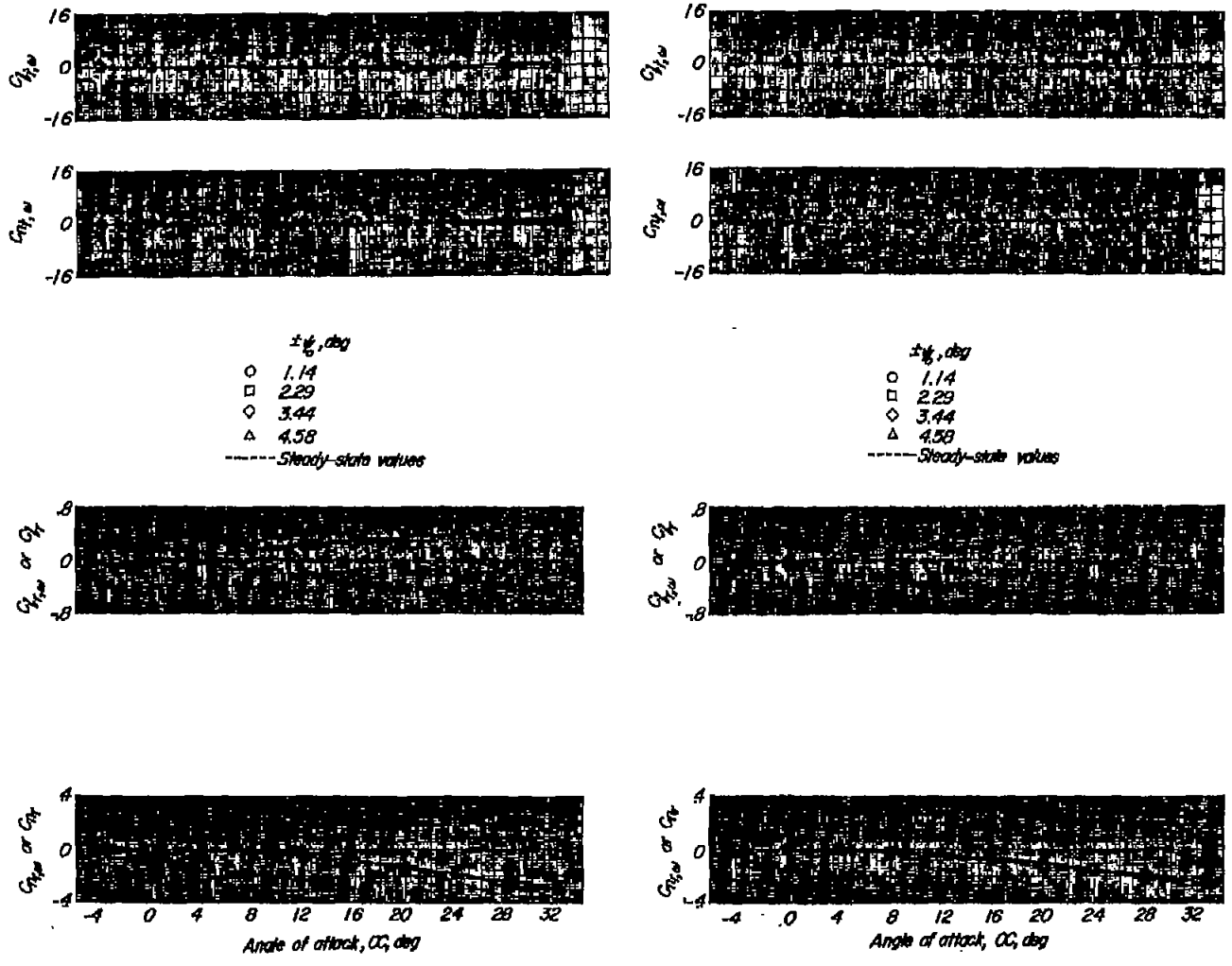

(c) $\frac{\omega b}{2V} = 0.12$.

(d) $\frac{\omega b}{2V} = 0.16$.

Figure 8.- Continued.

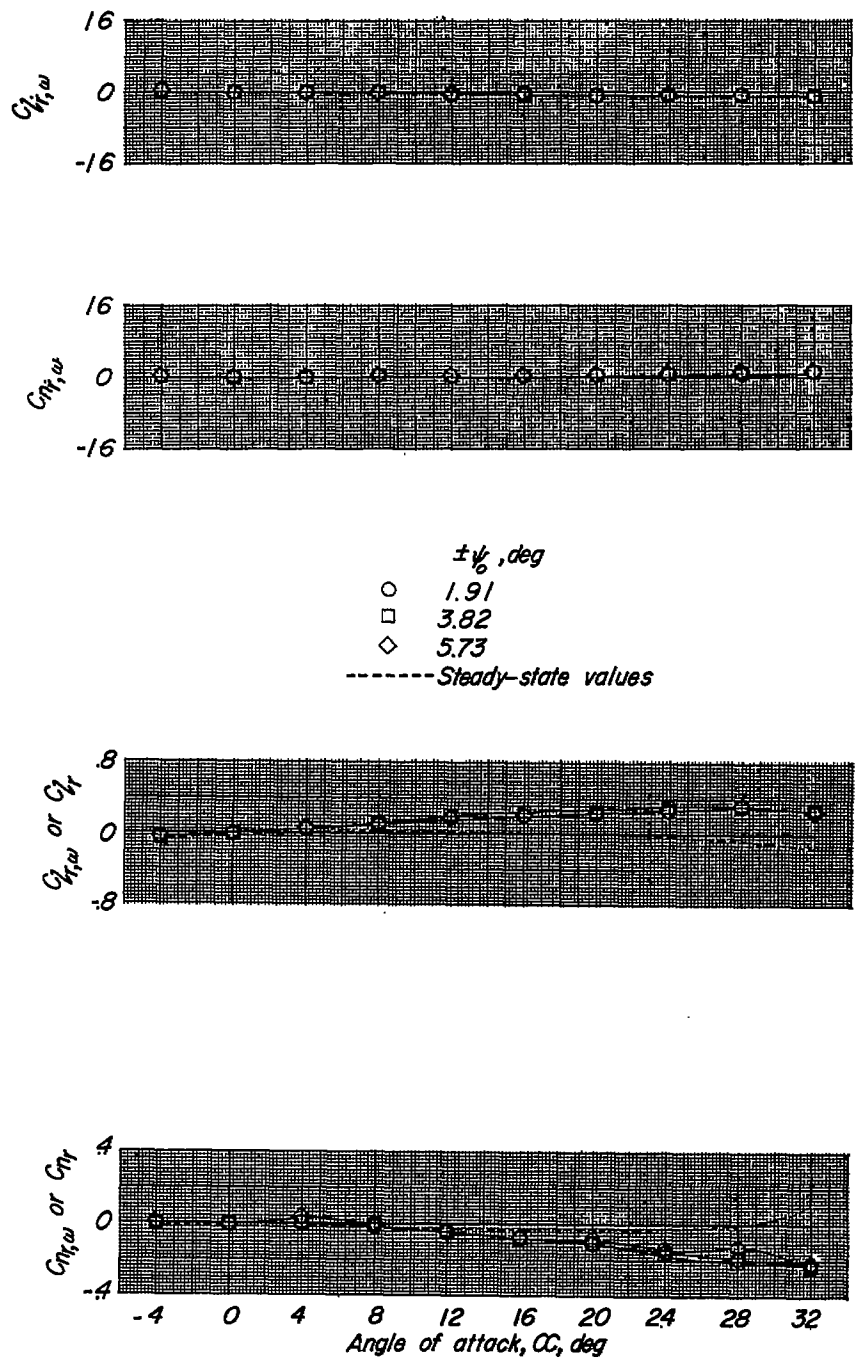

(e) $\frac{\omega b}{2V} = 0.20$.

Figure 8.- Concluded.

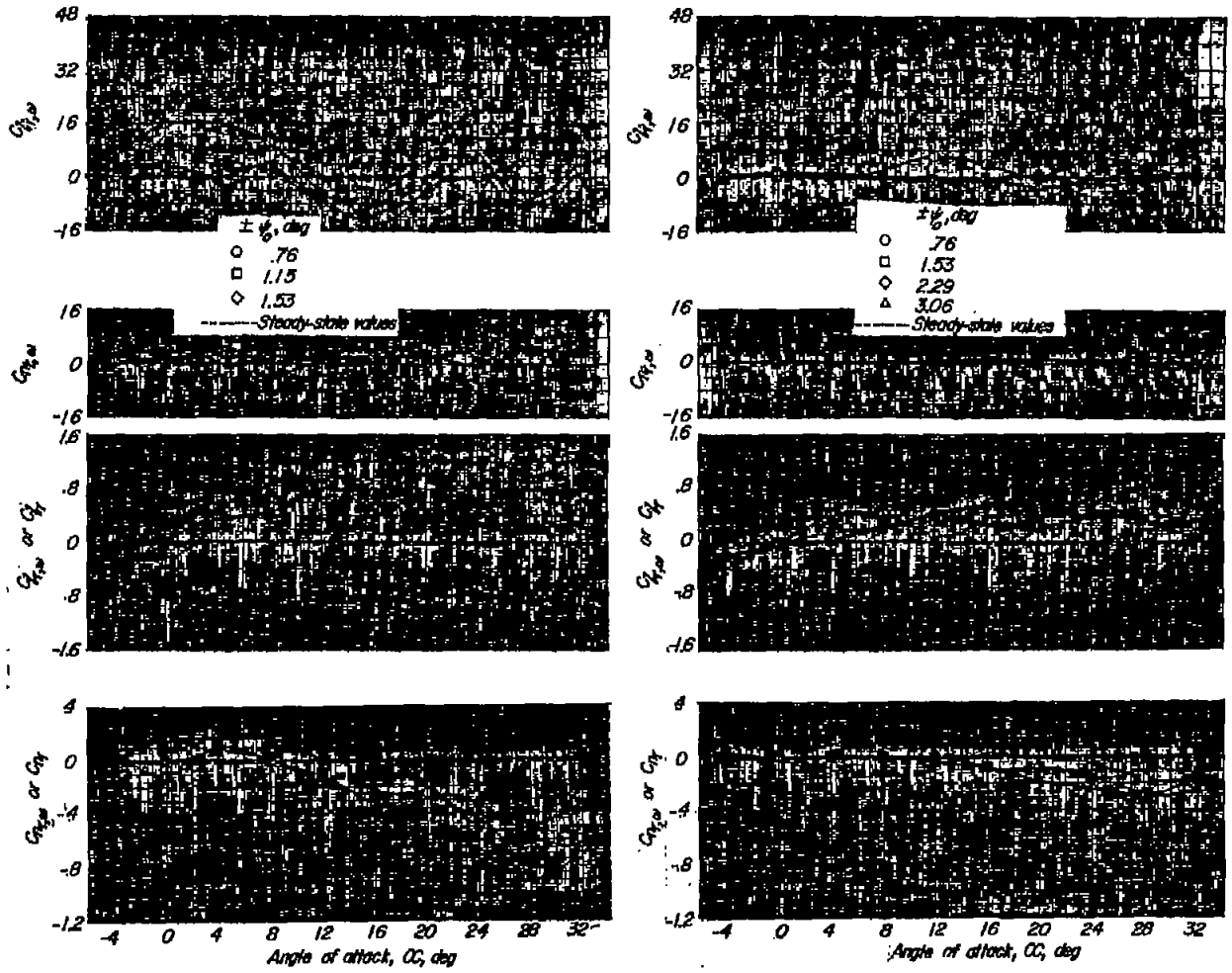

(a) $\frac{\omega b}{2V} = 0.04$.

(b) $\frac{\omega b}{2V} = 0.08$.

Figure 9.- Stability derivatives for the 45° swept wing measured during oscillation.

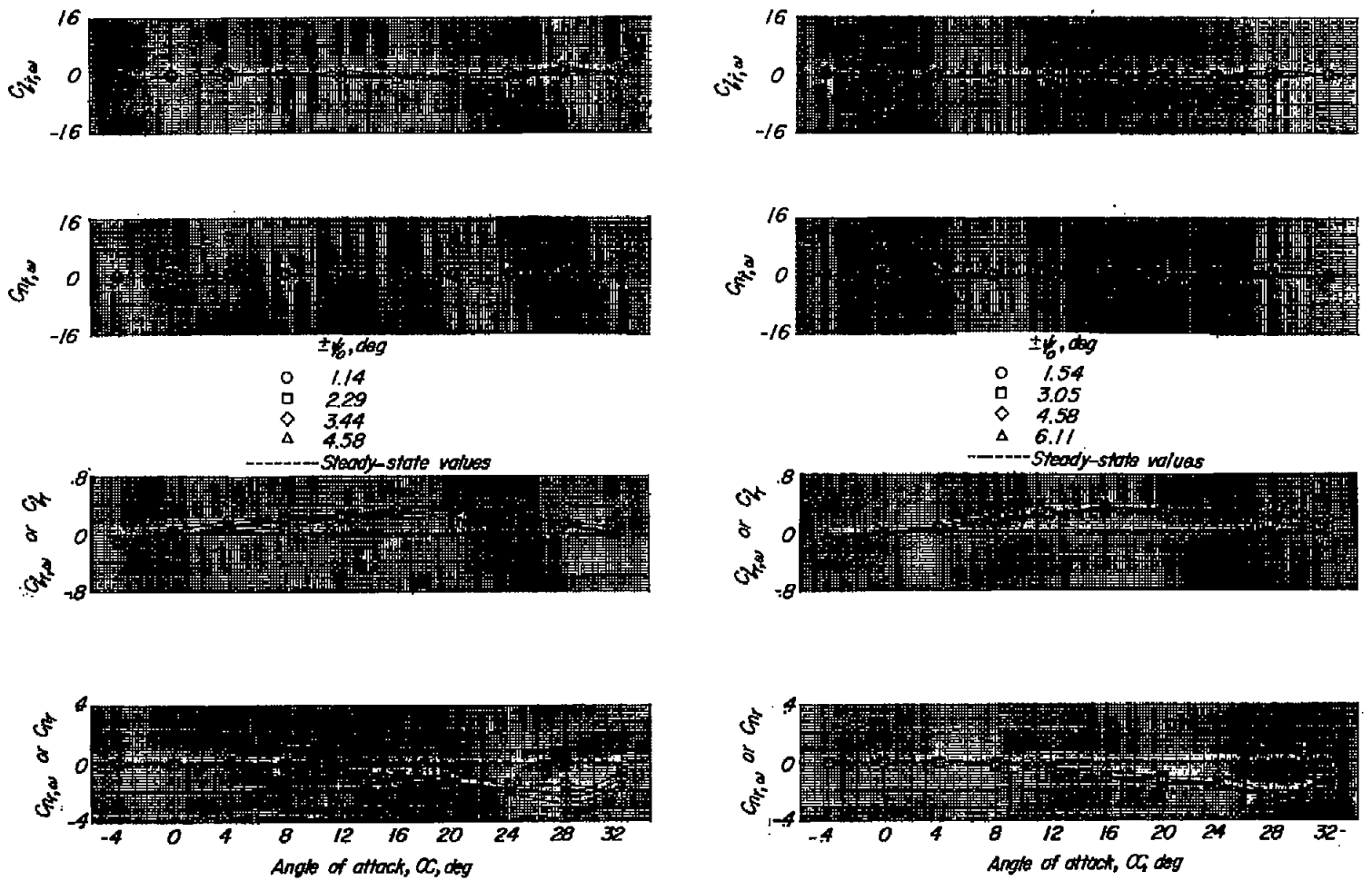

(c) $\frac{\omega b}{2V} = 0.12$.

(d) $\frac{\omega b}{2V} = 0.16$.

Figure 9.- Continued.

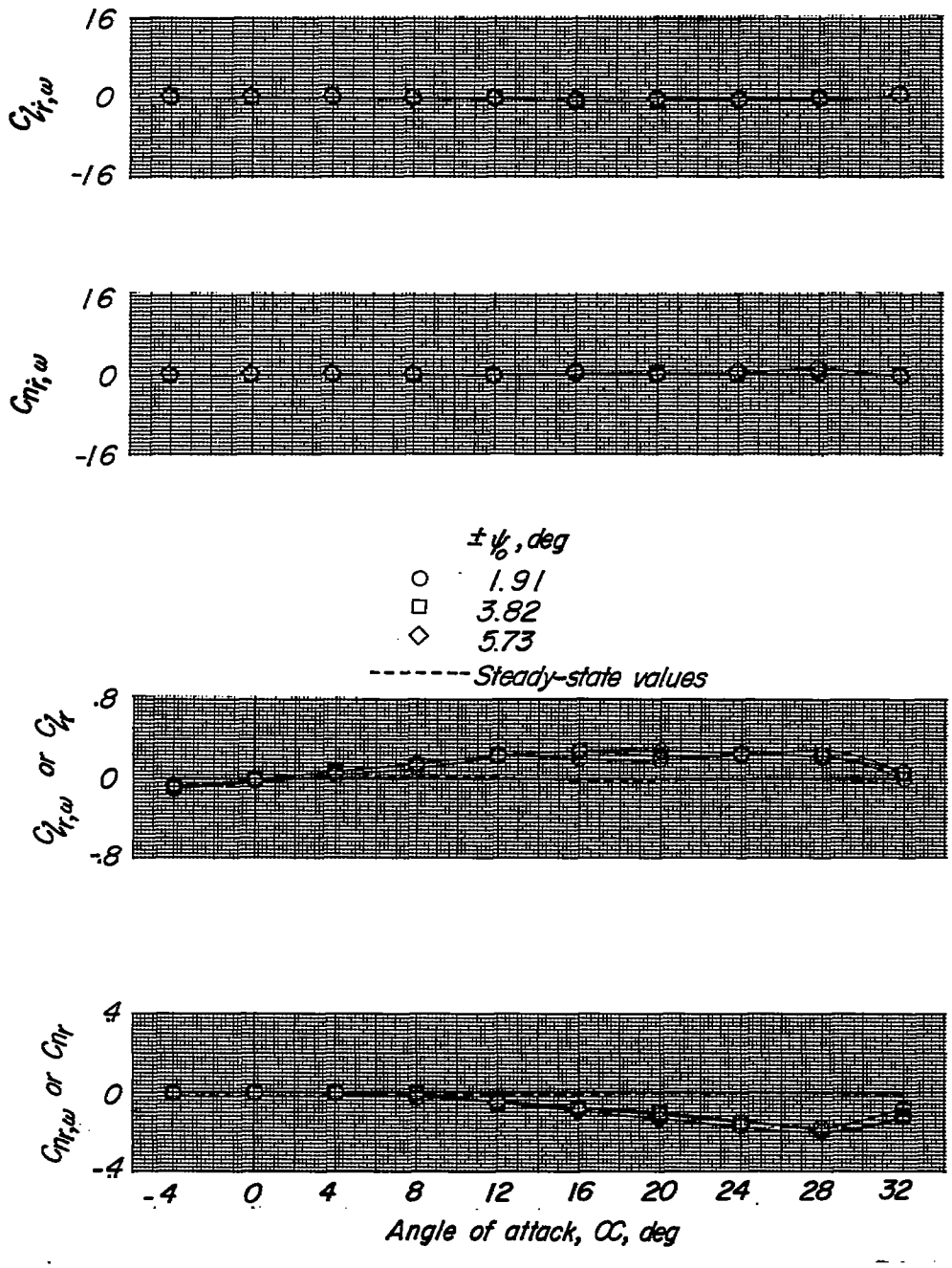

(e) $\frac{\omega b}{2V} = 0.20$.

Figure 9.- Concluded.

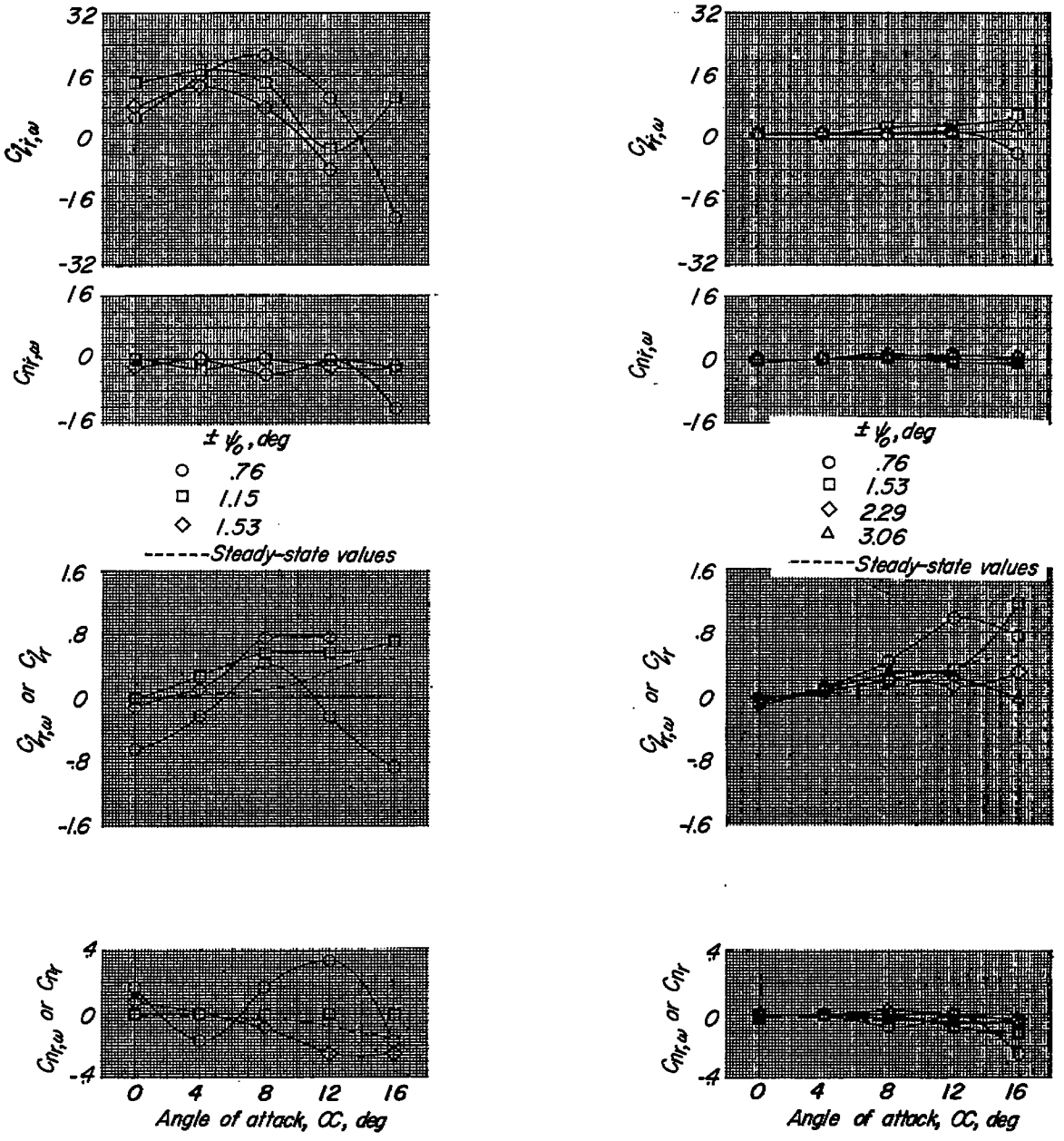

(a) $\frac{\omega b}{2V} = 0.04$.

(b) $\frac{\omega b}{2V} = 0.08$.

Figure 10.- Stability derivatives for the unswept wing measured during oscillation.

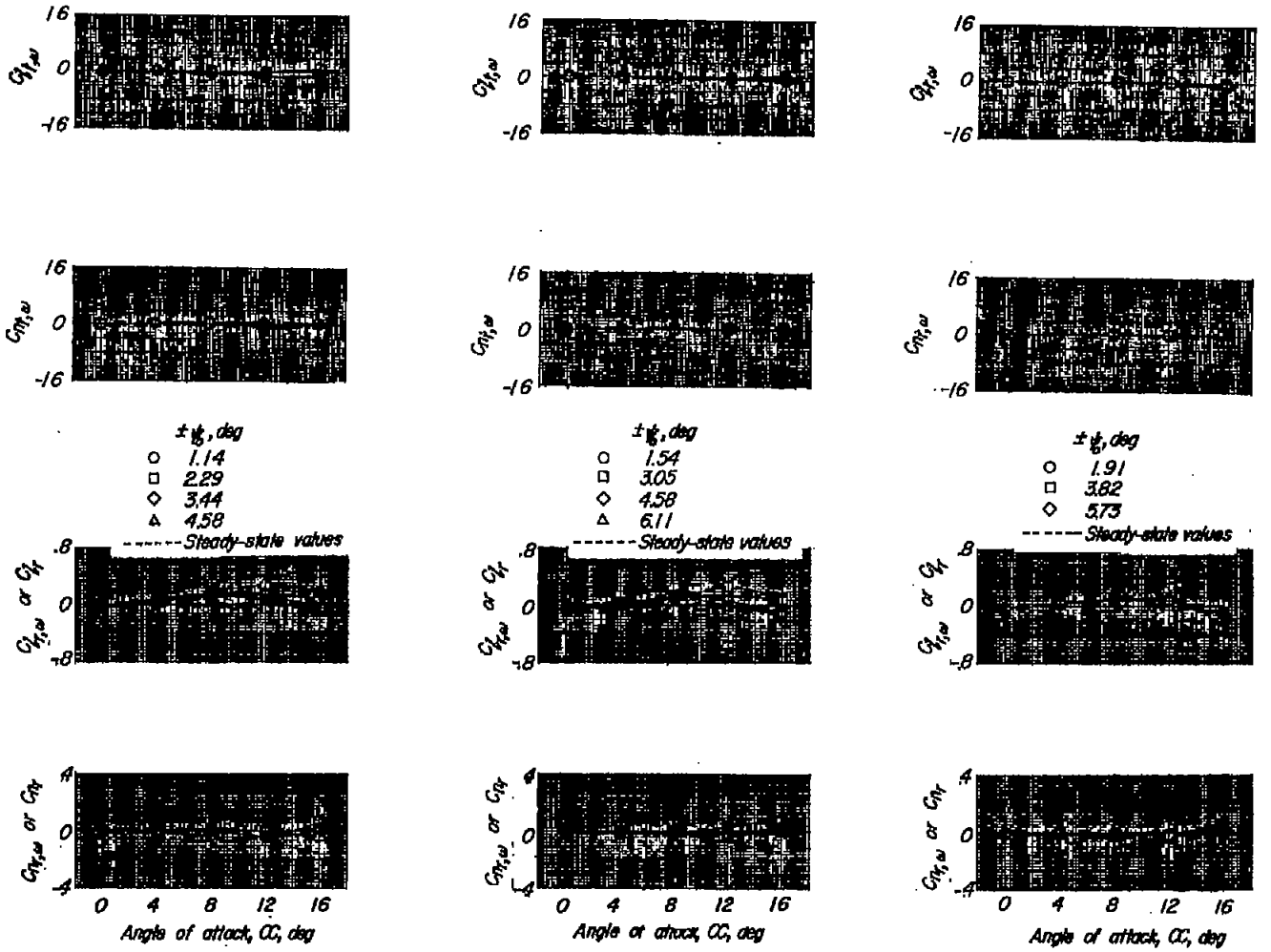

(c) $\frac{\omega b}{2V} = 0.12$.

(d) $\frac{\omega b}{2V} = 0.16$.

(e) $\frac{\omega b}{2V} = 0.20$.

Figure 10.- Concluded.

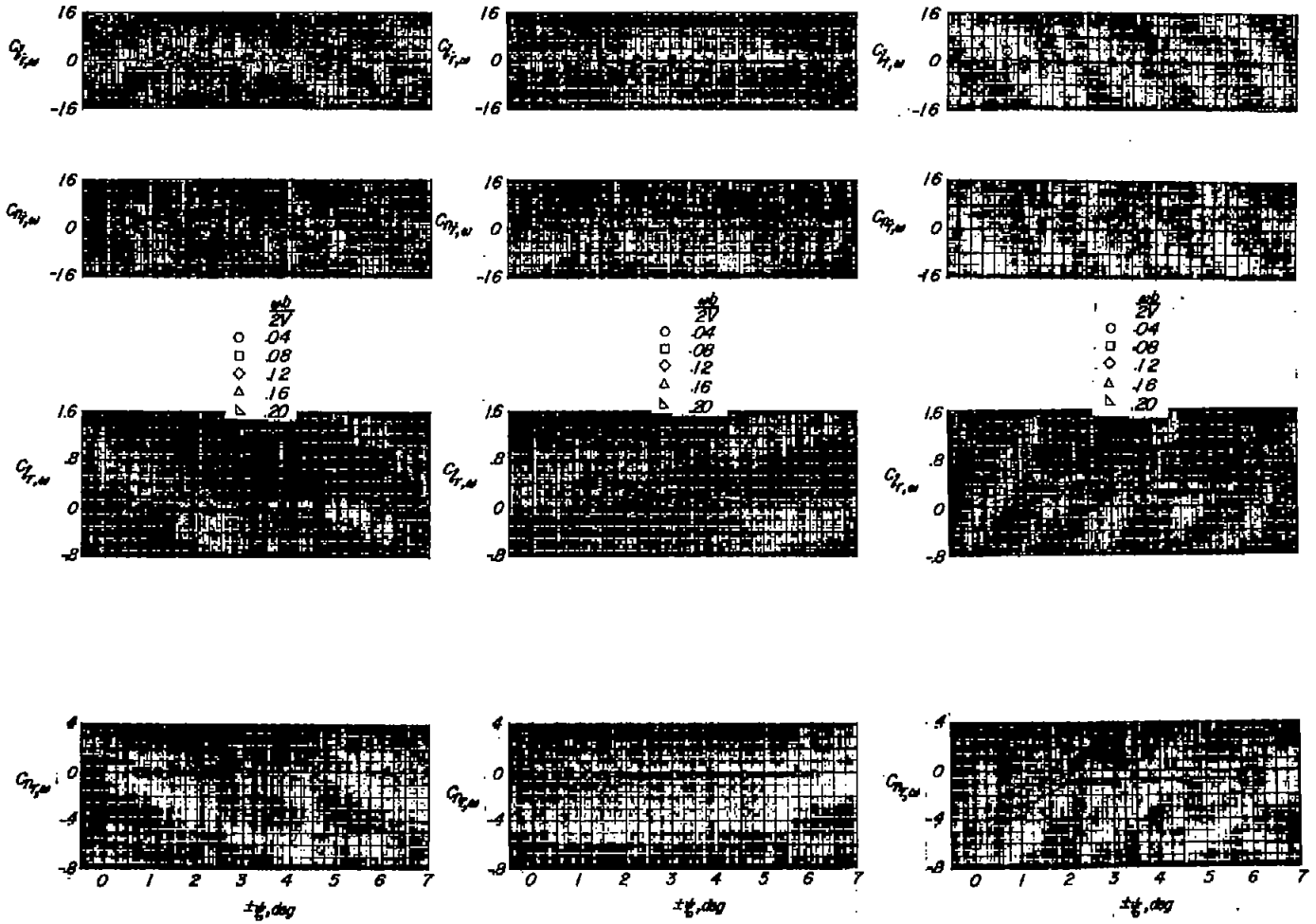

(a) $\alpha = 0^\circ$. (b) $\alpha = 8^\circ$. (c) $\alpha = 12^\circ$.

Figure 11.- Effect of amplitude on stability derivatives of the 60° triangular wing measured during oscillation.

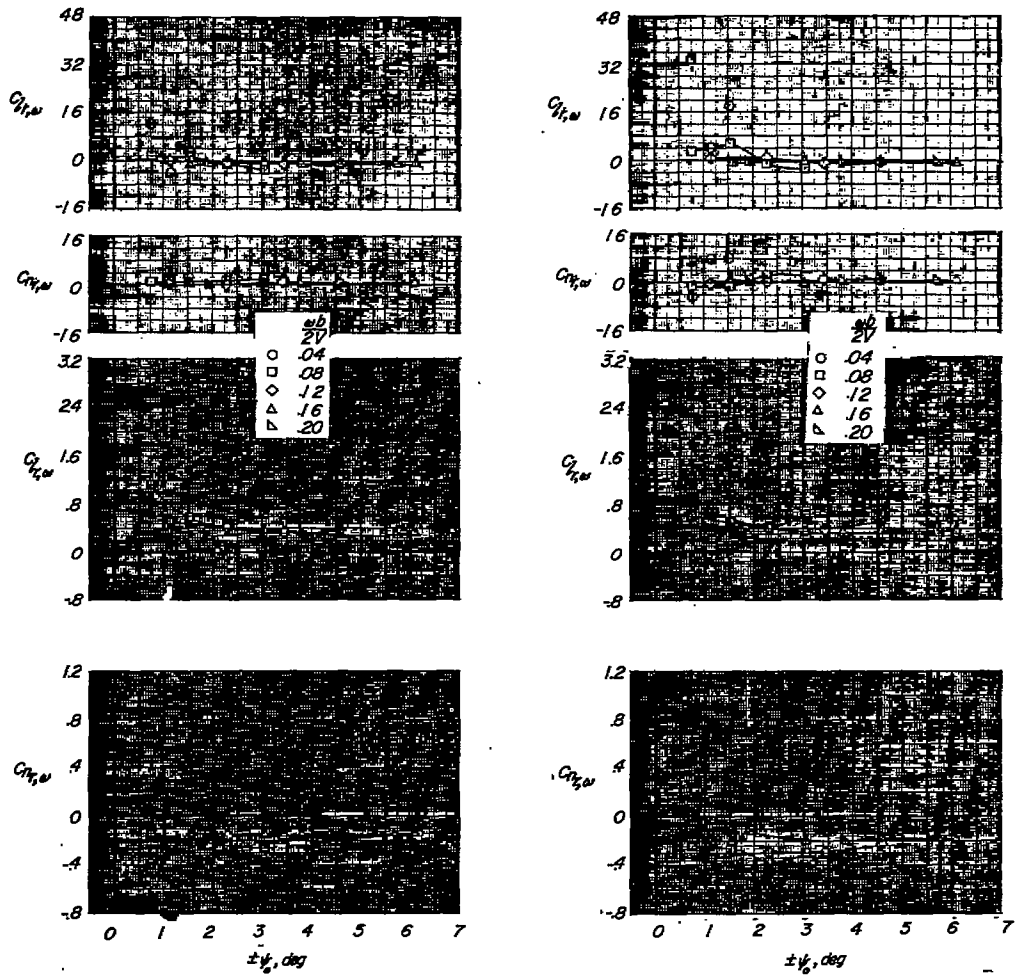

(d) $\alpha = 24^\circ$.

(e) $\alpha = 28^\circ$.

Figure 11.- Concluded.

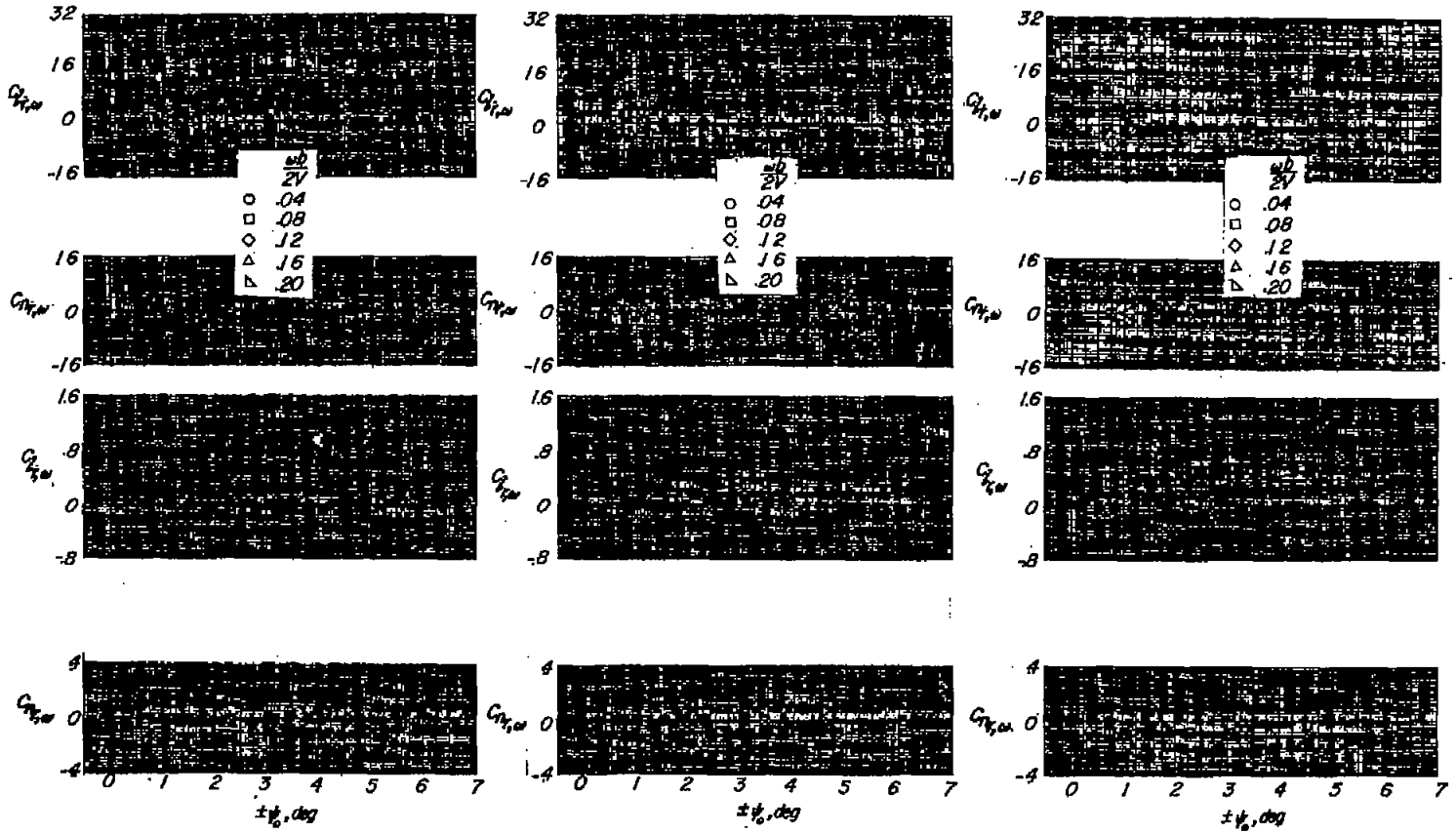

(a) $\alpha = 0^\circ$. (b) $\alpha = 8^\circ$. (c) $\alpha = 16^\circ$.

Figure 12.- Effect of amplitude on stability derivatives of the 45° swept wing measured during oscillation.

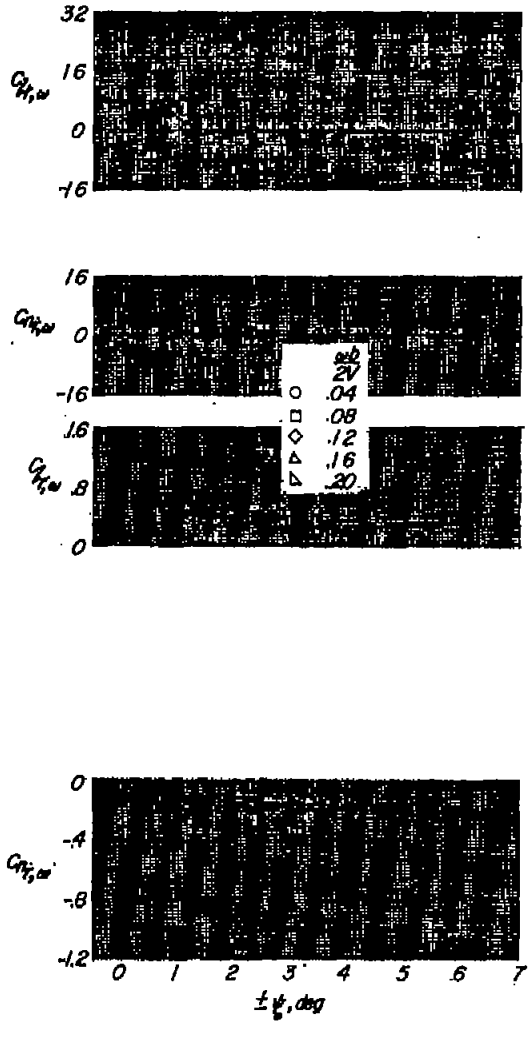

(d) $\alpha = 24^\circ$.

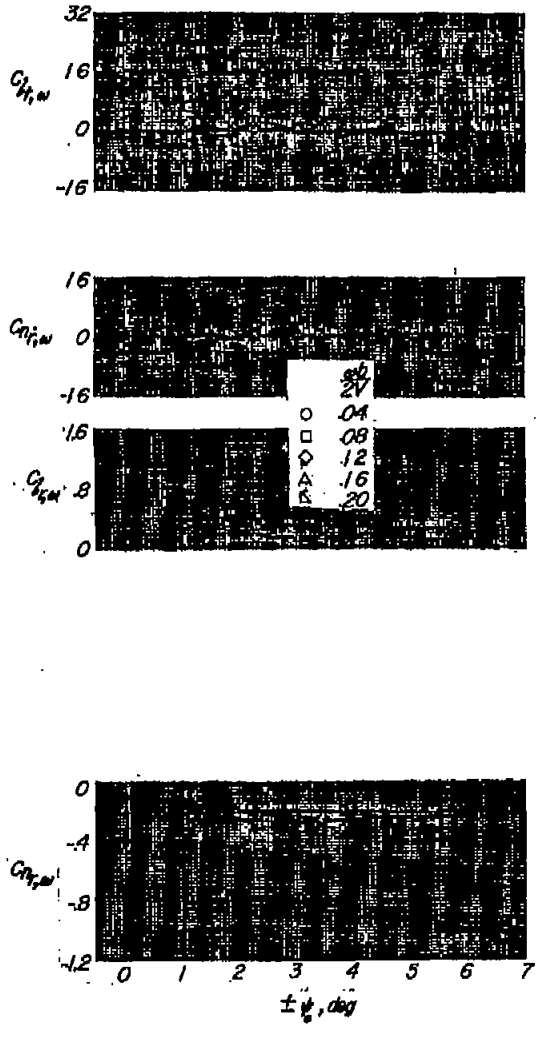

(e) $\alpha = 28^\circ$.

Figure 12.- Concluded.

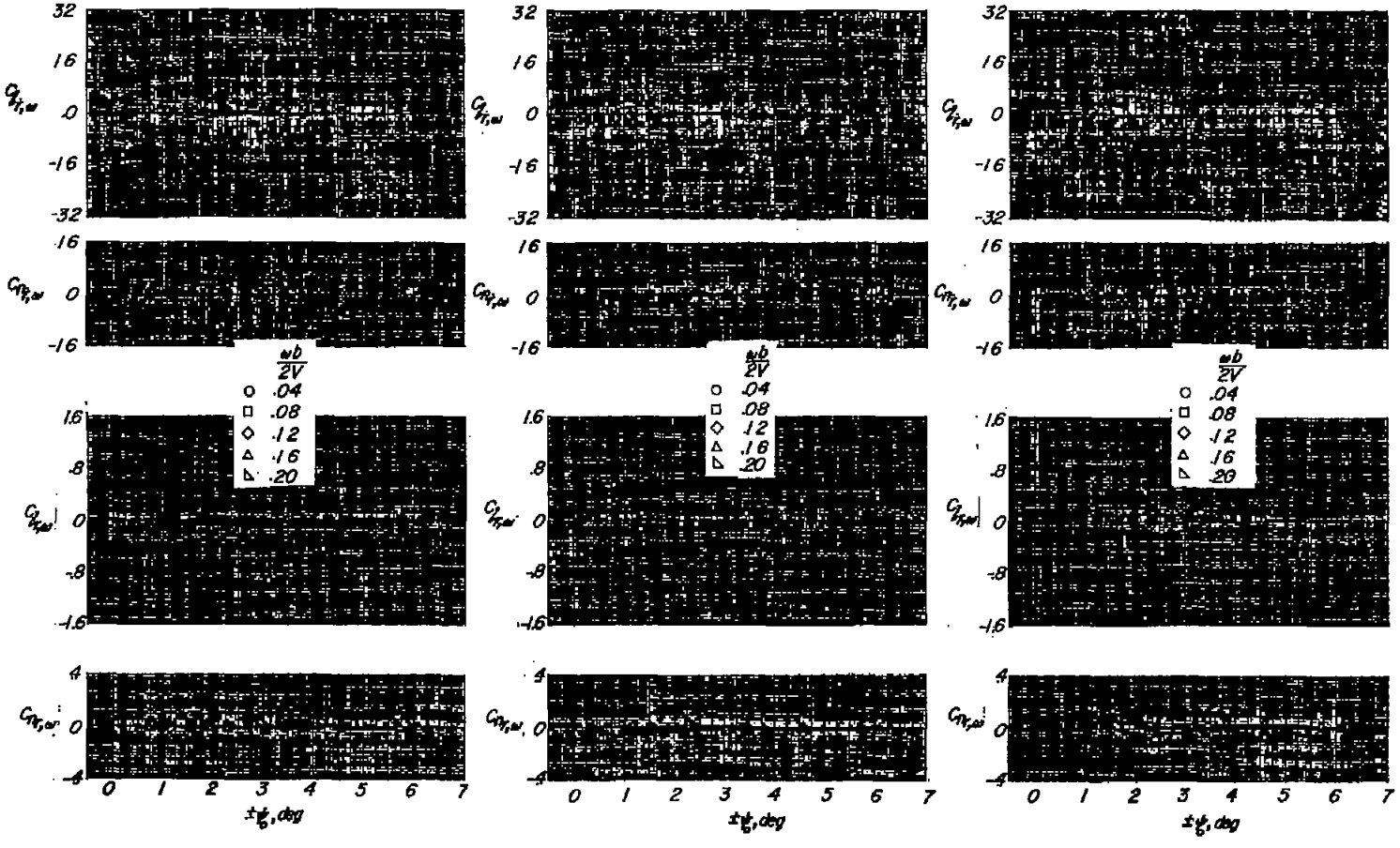

(a) $\alpha = 0^\circ$. (b) $\alpha = 8^\circ$. (c) $\alpha = 16^\circ$.

Figure 13.- Effect of amplitude on stability derivatives of the unswept wing measured during oscillation.

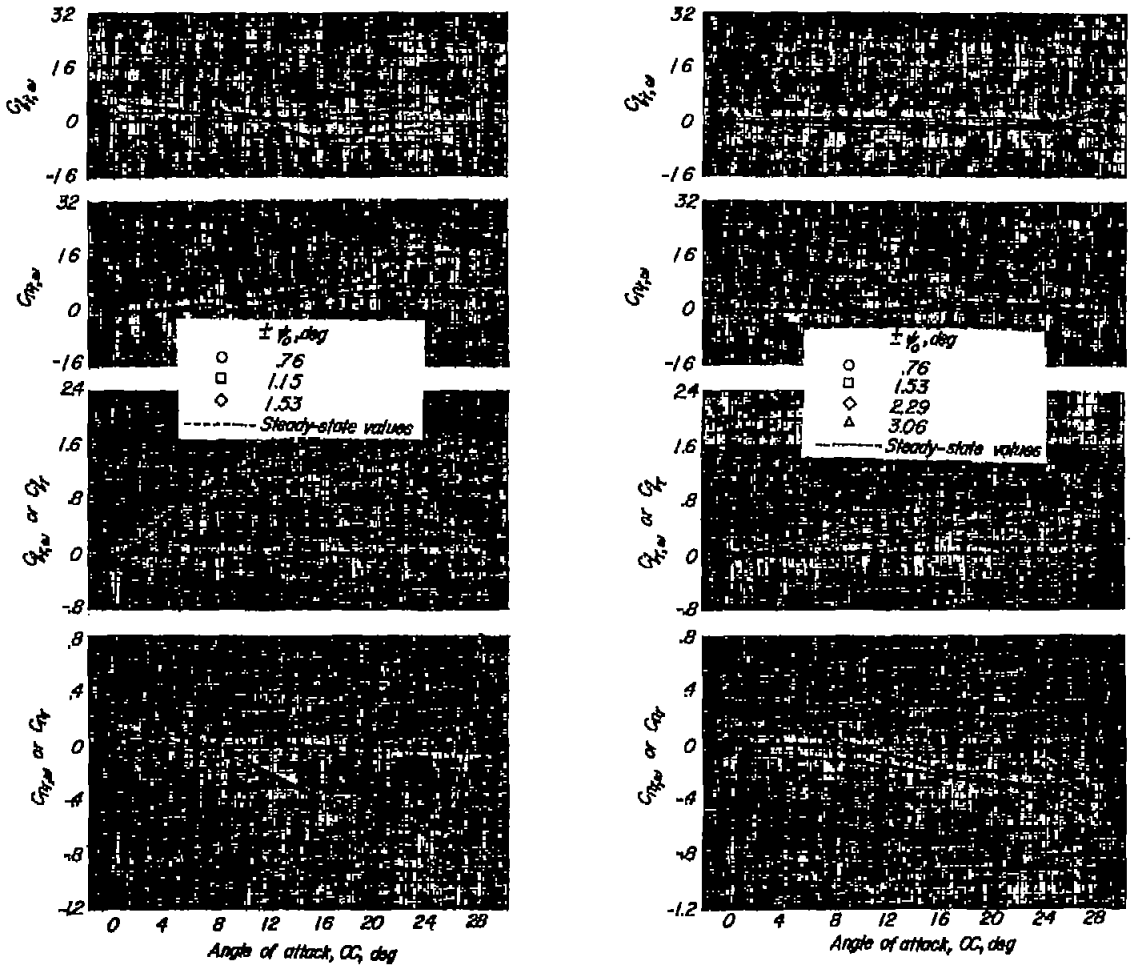

(a) $\frac{\omega b}{2V} = 0.04$.

(b) $\frac{\omega b}{2V} = 0.08$.

Figure 14.- Stability derivatives of the triangular-wing—fuselage configuration measured during oscillation.

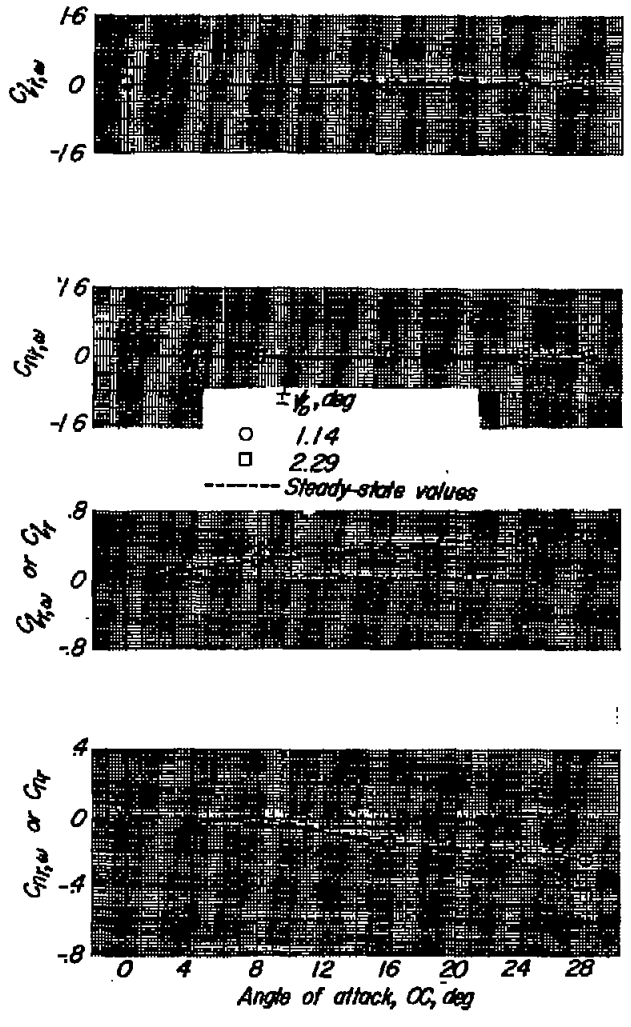

(c) $\frac{\omega b}{2V} = 0.12$.

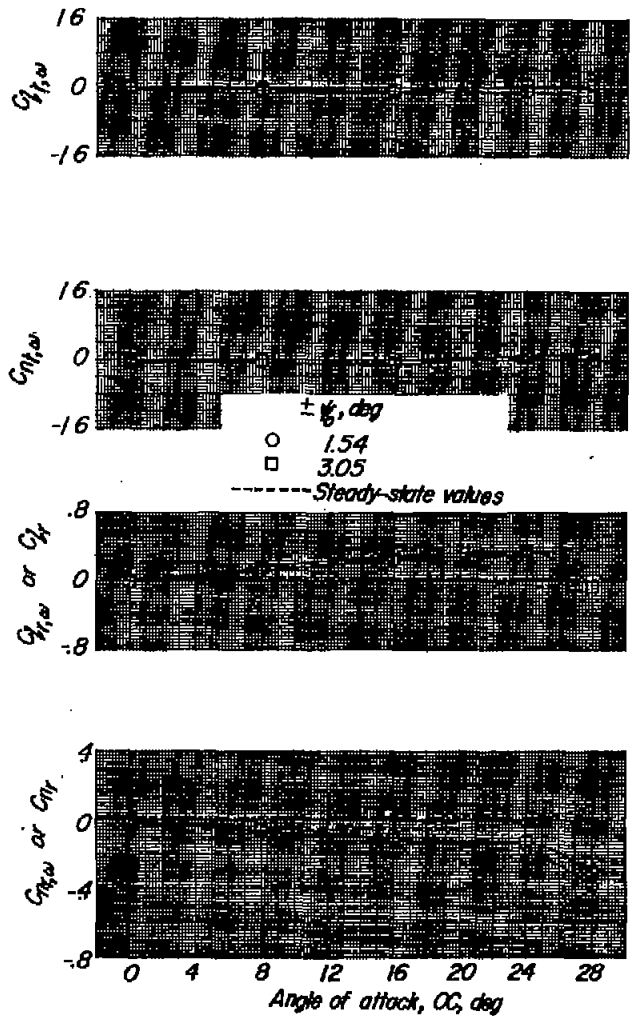

(d) $\frac{\omega b}{2V} = 0.16$.

Figure 14.- Concluded.

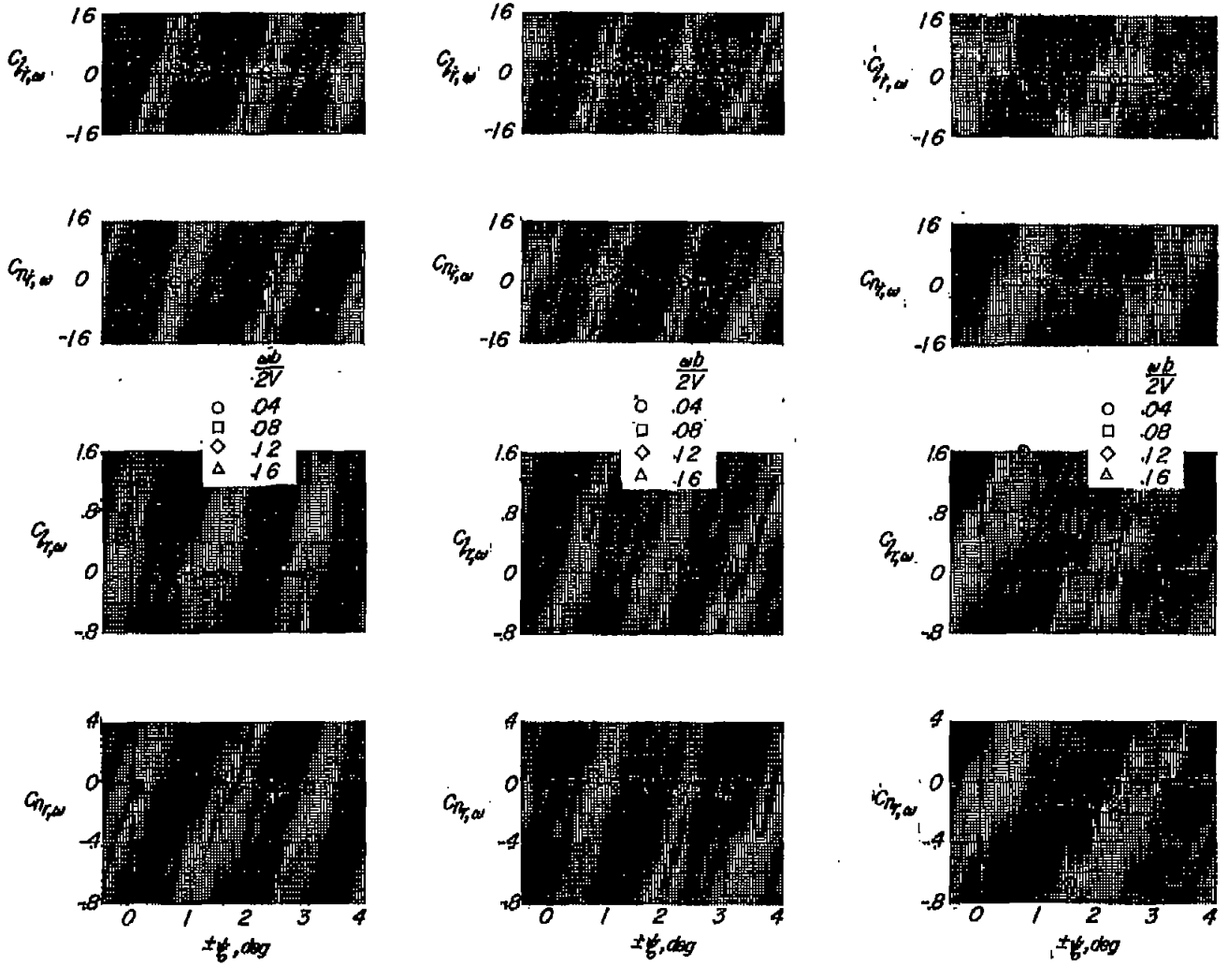

(a) $\alpha = 0^\circ$. (b) $\alpha = 8^\circ$. (c) $\alpha = 16^\circ$.

Figure 15.- Effect of amplitude on stability derivatives of the triangular-wing—fuselage configuration measured during oscillation.

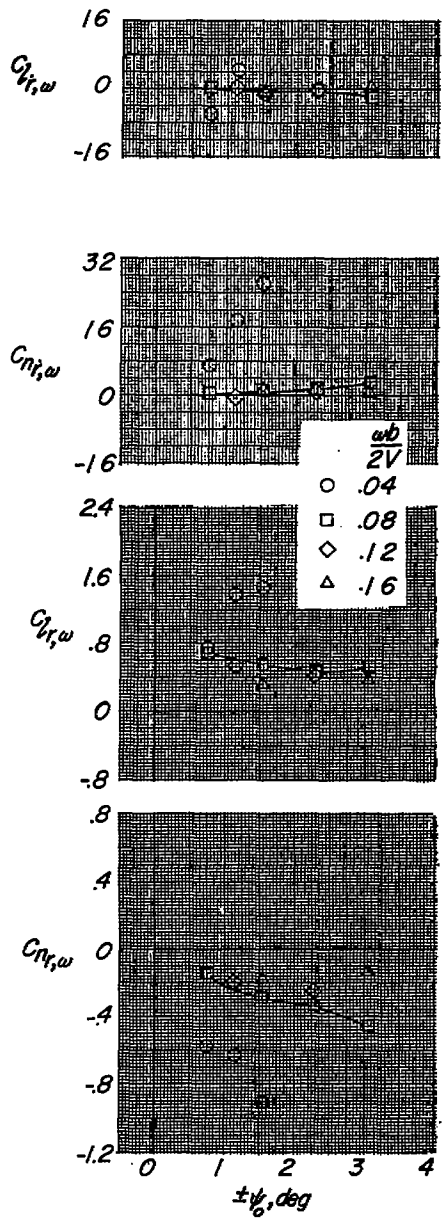

(d) $\alpha = 24^\circ$.

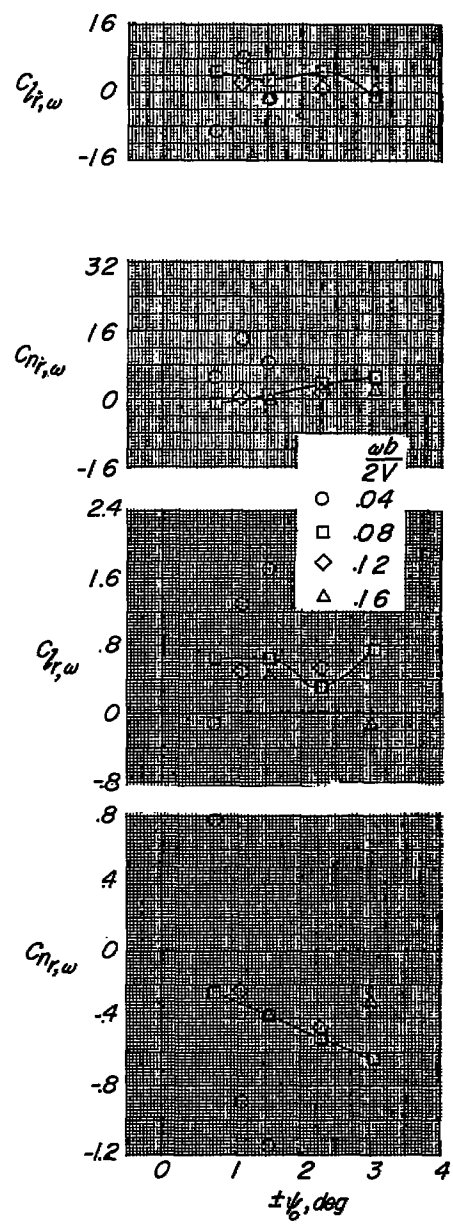

(e) $\alpha = 28^\circ$.

Figure 15.- Concluded.

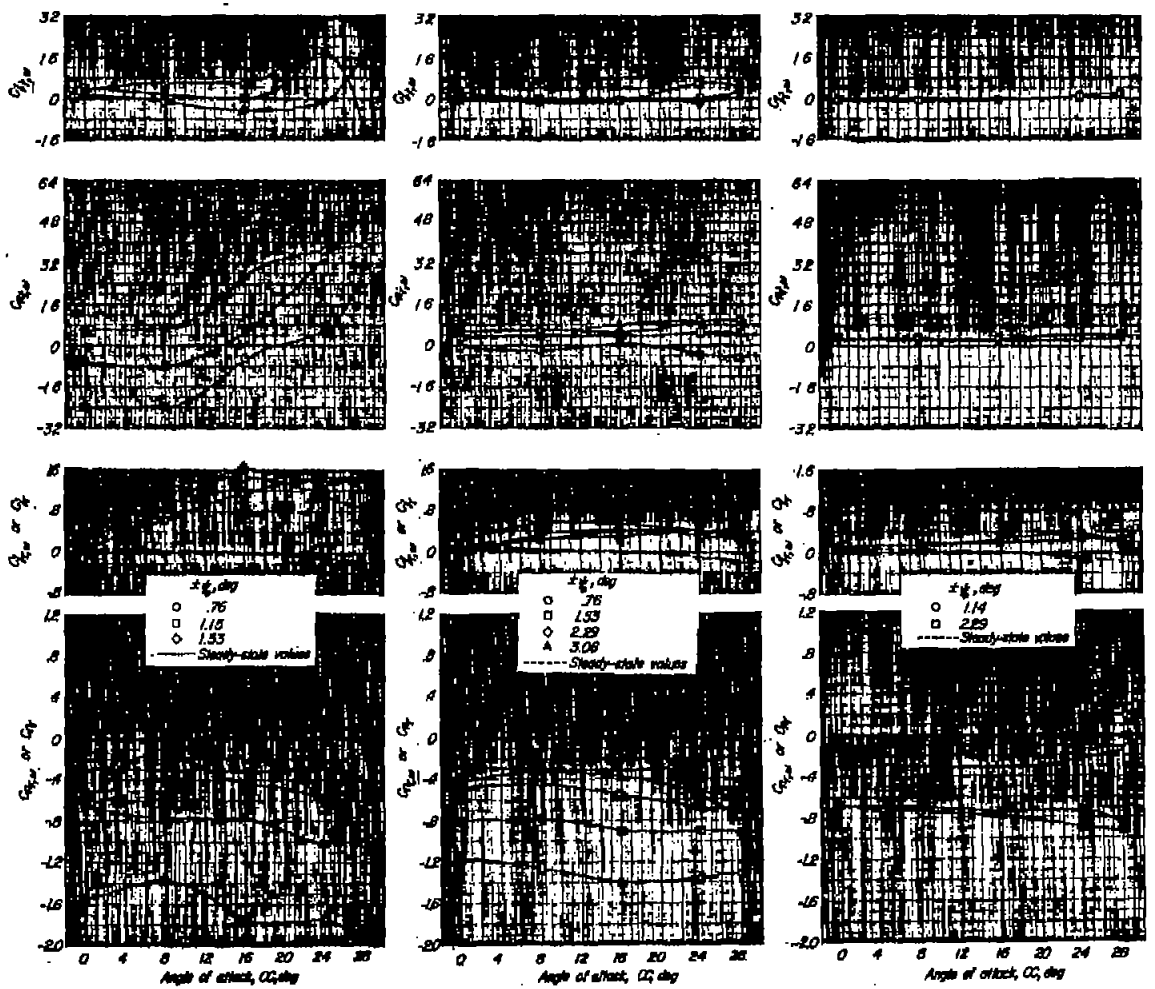

(a) $\frac{\omega b}{2V} = 0.04$. (b) $\frac{\omega b}{2V} = 0.08$. (c) $\frac{\omega b}{2V} = 0.12$.

Figure 16.- Stability derivatives of the wing-fuselage-tail configuration measured during oscillation.

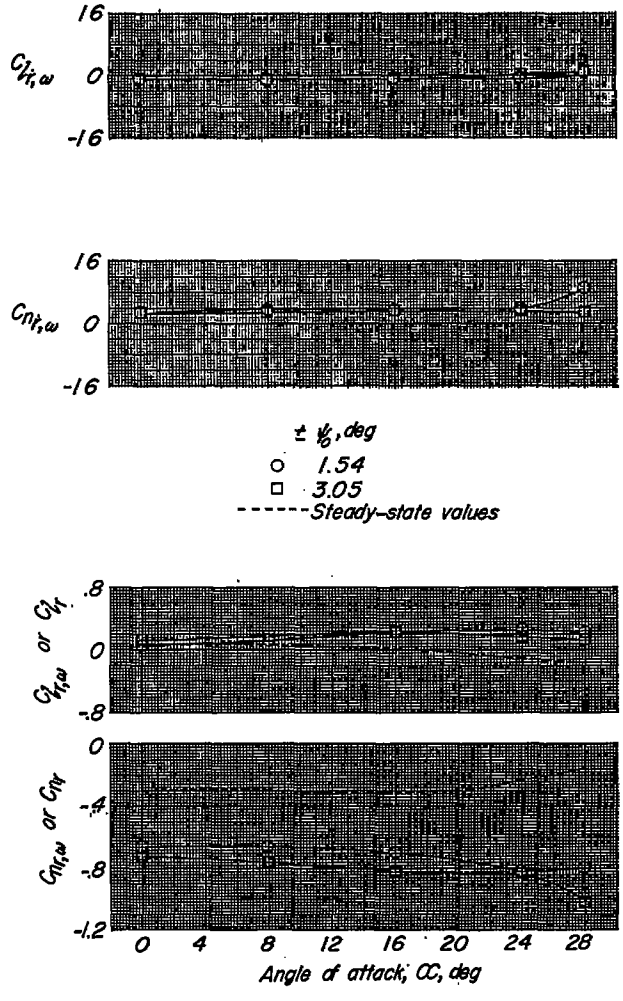

(d) $\frac{\omega b}{2V} = 0.16$.

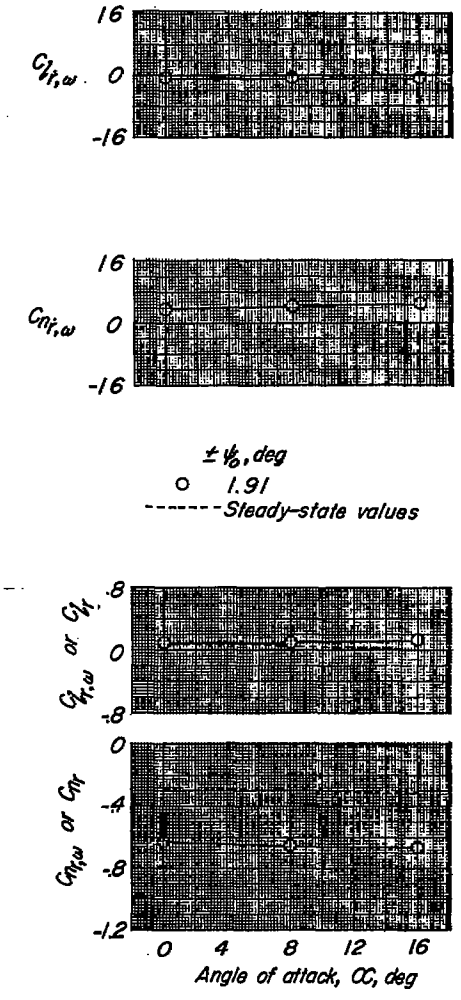

(e) $\frac{\omega b}{2V} = 0.20$.

Figure 16.- Concluded.

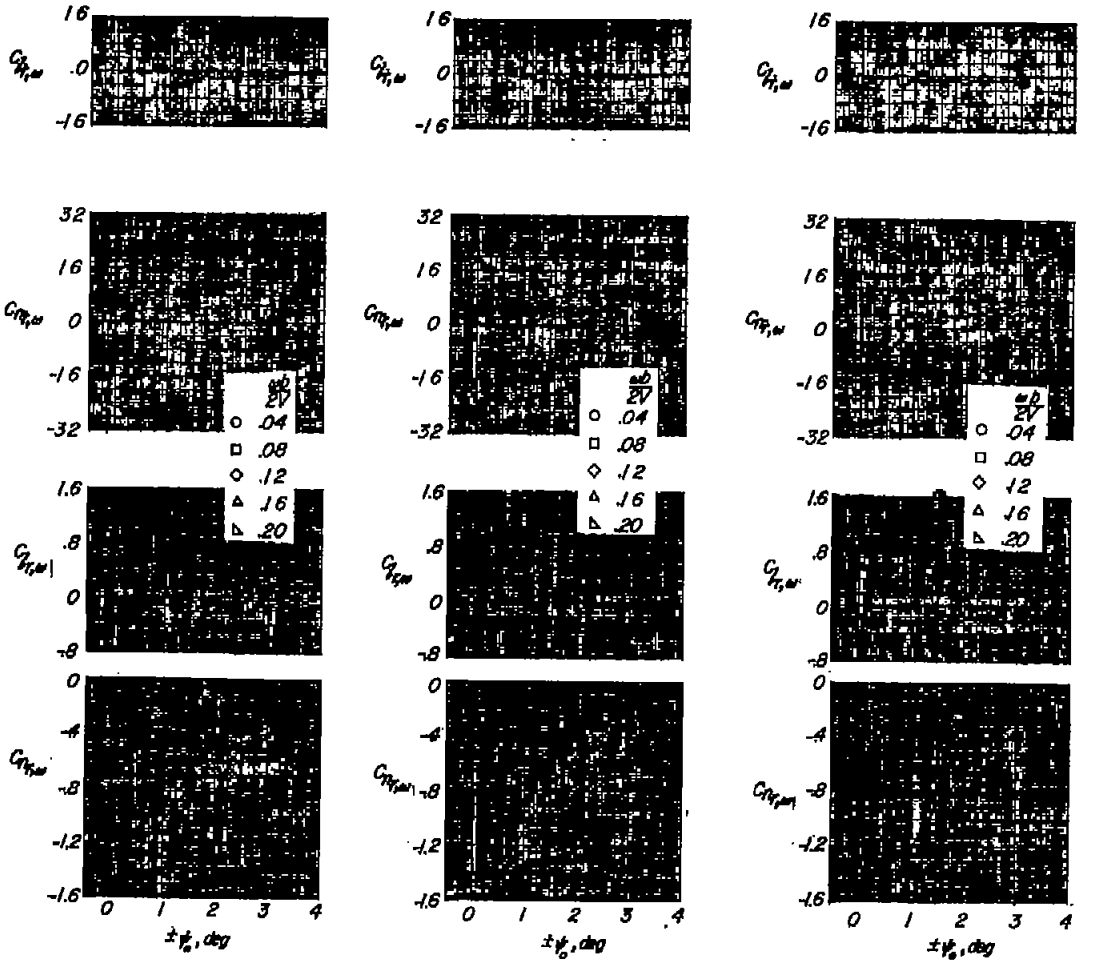

(a) $\alpha = 0^\circ$. (b) $\alpha = 8^\circ$. (c) $\alpha = 16^\circ$.

Figure 17.- Effect of amplitude on stability derivatives of the triangular-wing—fuselage configuration with tail measured during oscillation.

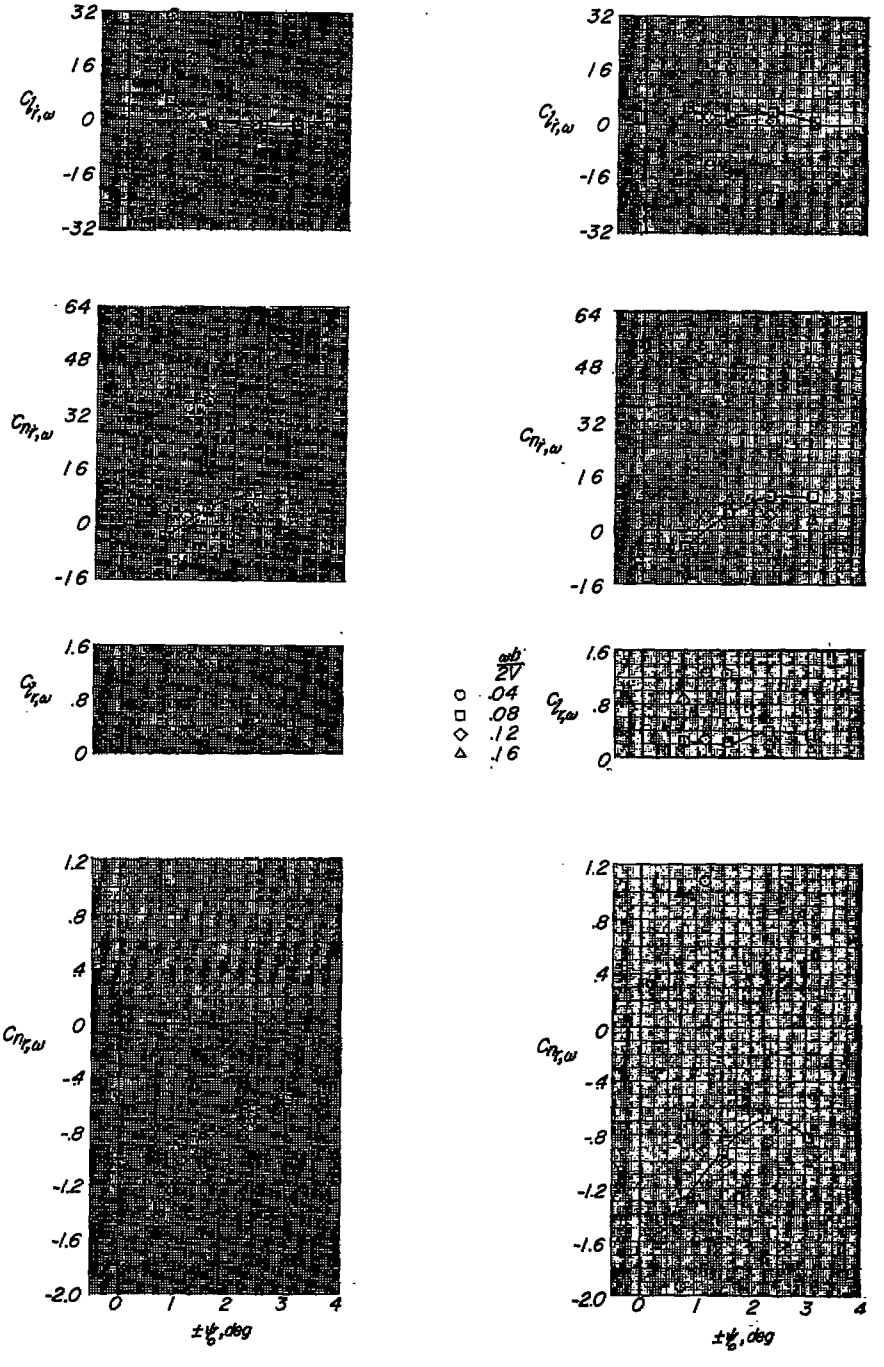

(d) $\alpha = 24^\circ$.

(e) $\alpha = 28^\circ$.

Figure 17.- Concluded.

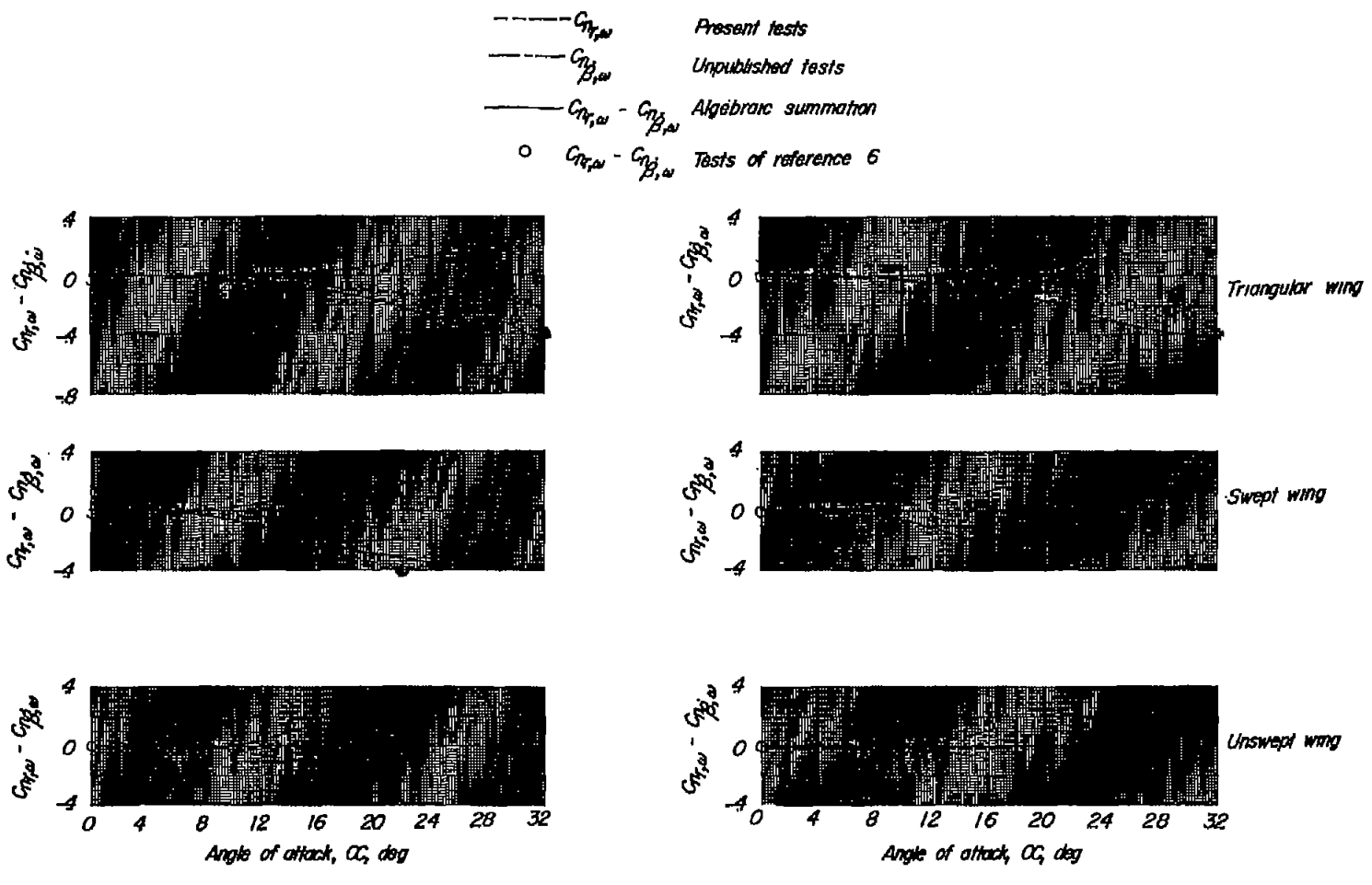

(a) $\Psi_o = \pm 2^\circ$.

(b) $\Psi_o = \pm 4^\circ$.

Figure 18.- Comparison of the individual and combination derivatives making up the damping in yaw.

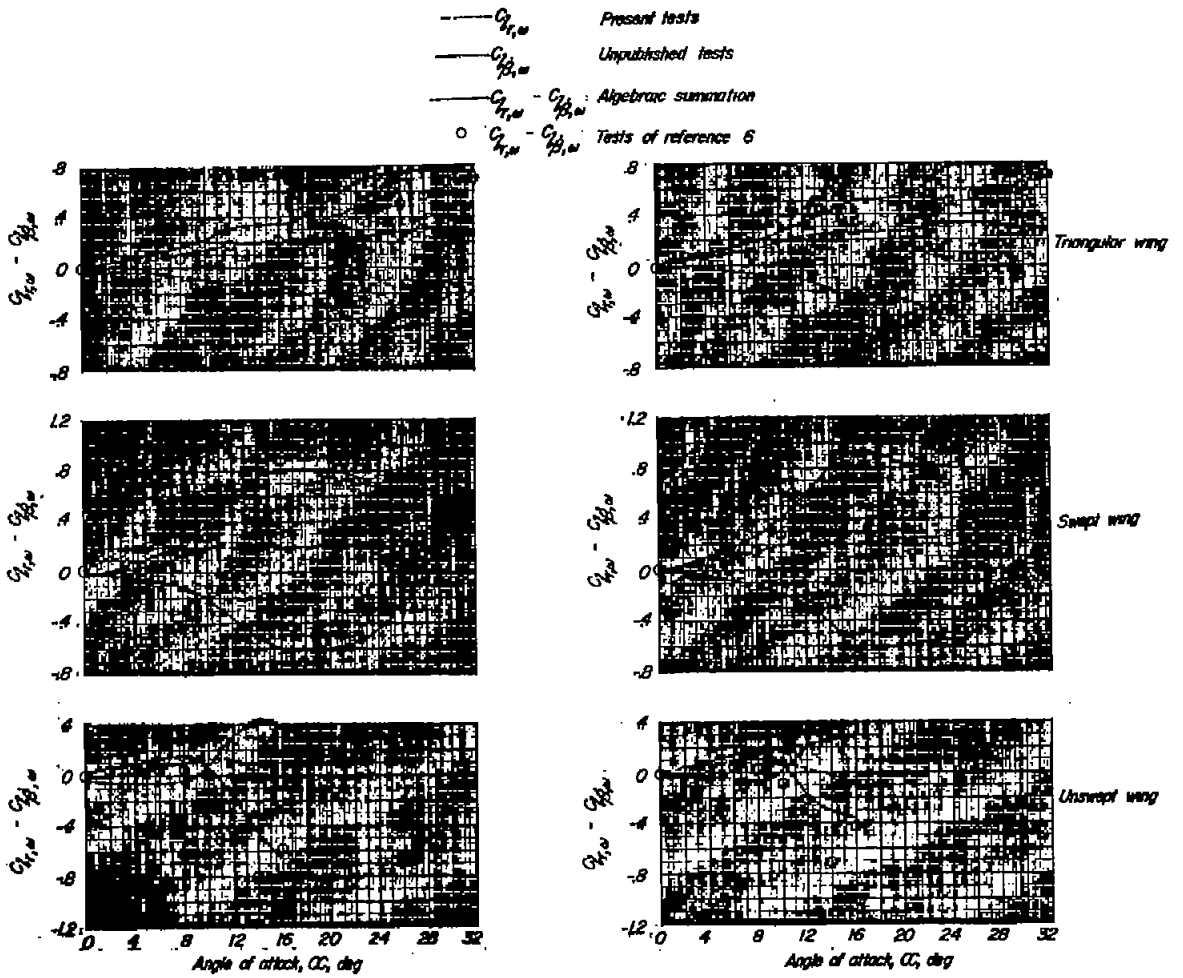

(a) $\psi_o = \pm 2^o$.

(b) $\psi_o = \pm 4^o$.

Figure 19.- Comparison of the individual and combination derivatives making up the rolling moment due to yawing.

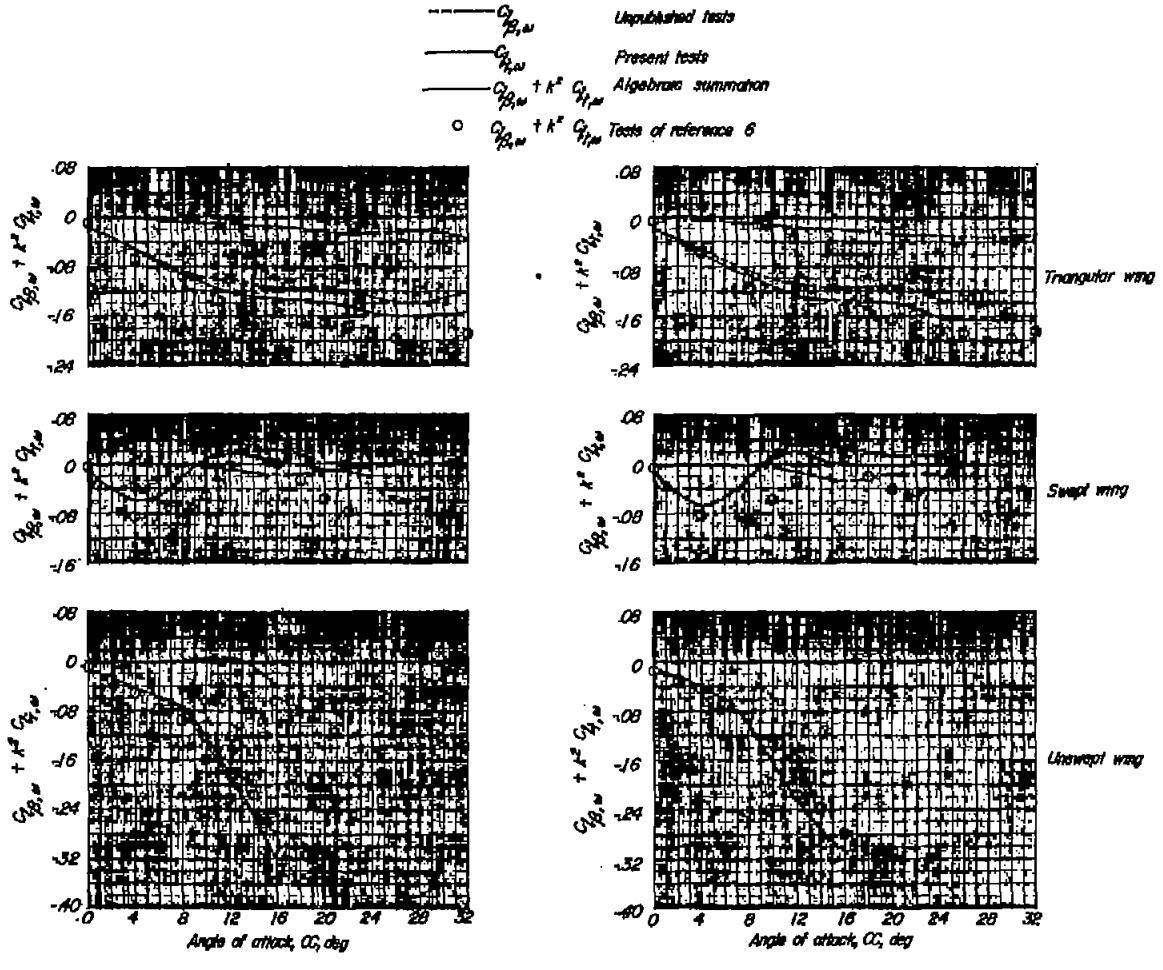

(a) $\psi_o = \pm 2^\circ$.

(b) $\psi_o = \pm 4^\circ$.

Figure 20.- Comparison of the individual and combination derivatives making up the effective dihedral.

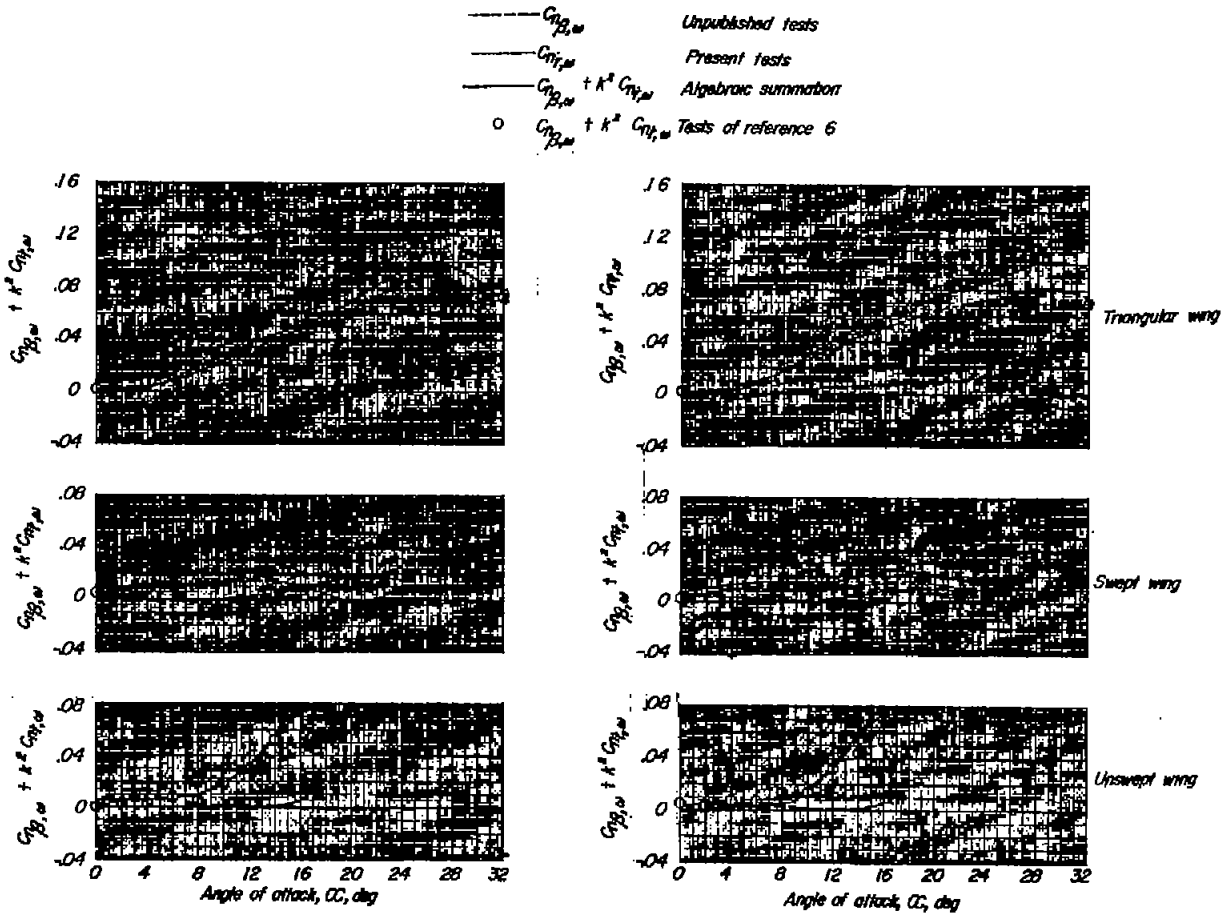

(a) $\Psi_o = \pm 2^o$.

(b) $\Psi_o = \pm 4^o$.

Figure 21.- Comparison of the individual and combination derivatives making up the directional stability.